Title	Abrupt Holocene ice-sheet thinning along the southern Soya Coast,Lützow-Holm Bay, East Antarctica, revealed by glacial geomorphology and surface exposure dating
Authors	Moto Kawamata, Yusuke Suganuma, Koichiro Doi, Keiji Misawa, Motohiro Hirabayashi, Akihisa Hattori, Takanobu Sawagaki
Citation	Quaternary Science Reviews, 247, 1-19, 2020
Issue Date	2020-11-1
Type	Journal Article
URL	htthttps://doi.org/10.1016/j.quascirev.2020.106540
Right	
Textversion	publisher

Abrupt Holocene ice-sheet thinning along the southern Soya Coast, Lützow-Holm Bay, East Antarctica, revealed by glacial geomorphology and surface exposure dating

Moto Kawamata [a, *], Yusuke Suganuma [a, b], Koichiro Doi [a, b], Keiji Misawa [a, b], Motohiro Hirabayashi [b], Akihisa Hattori [a], Takanobu Sawagaki [c]

[a] Department of Polar Science, School of Multidisciplinary Sciences, The Graduate University for Advanced Studies (SOKENDAI), Japan
[b] National Institute of Polar Research, Tokyo, Japan
[c] Faculty of Social Sciences, Hosei University, Tokyo, Japan

A B S T R A C T

Geological reconstruction of the retreat history of the East Antarctic Ice Sheet (EAIS) since the Last Glacial Maximum (LGM) is essential for understanding the response of the ice sheet to global climatic change and the mechanisms of retreat, including a possible abrupt melting event. Such information is key for constraining climatic and ice-sheet models that are used to predict future Antarctic Ice Sheet AIS melting. However, data required to make a detailed reconstruction of the history of the EAIS involving changes in its thickness and lateral extent since the LGM remain sparse. Here, we present a new detailed ice-sheet history for the southern Soya Coast, Lützow-Holm Bay, East Antarctica, based on geomorphological observations and surface exposure ages. Our results demonstrate that the ice sheet completely covered the highest peak of Skarvsnes (400 m a.s.l.) prior to ~9 ka and retreated eastward by at least 10 km during the Early to Mid-Holocene (ca. 9 to 5 ka). The timing of the abrupt ice-sheet thinning and retreat is consistent with the intrusion of modified Circumpolar Deep Water (mCDW) into deep submarine valleys in Lützow-Holm Bay, as inferred from fossil foraminifera records of marine sediment cores. Thus, we propose that the mechanism of the abrupt thinning and retreat of the EAIS along the southern Soya Coast was marine ice-sheet instability caused by mCDW intrusion into deep submarine valleys. Such abrupt ice-sheet thinning and retreat with similar magnitude and timing have also been reported from Enderby Land, East Antarctica. Our findings suggest that abrupt thinning and retreat as a consequence of marine ice-sheet instability and intrusion of mCDW during the Early to Mid-Holocene may have led to rapid ice-surface lowering of hundreds of meters in East Antarctica.

1. Introduction

Accelerated ice-mass loss of the Antarctic Ice Sheet (AIS) has been reported through satellite measurements and oceanographic observations in recent decades (e.g., Jacobs et al., 2011; Rignot et al., 2011; Pritchard et al., 2012; Shepherd et al., 2012; Paolo et al., 2015; Rignot et al., 2019). The main processes of the mass loss of the AIS are considered to be calving and basal melting of ice shelves (e.g., Depoorter et al., 2013; Dinniman et al., 2016), with basal melting identified as a major contributor to the present ice-mass loss in

West Antarctica, especially in the Amundsen and Bellingshausen seas (e.g., Pritchard et al., 2012; Joughin et al., 2014; Paolo et al., 2015; Jenkins et al., 2018). A key process of the enhanced basal melting is thought to be inflow of modified Circumpolar Deep Water (mCDW) to the continental shelf (e.g., Thoma et al., 2008; Jacobs et al., 2011; Dinniman et al., 2012; Rignot et al., 2013; Liu et al., 2015; Nakayama et al., 2018). Thinning of ice shelves owing to basal melting is expected to have propagated into the continental ice sheet (Schoof, 2007; Golledge et al., 2012; Whitehouse et al., 2017) and to have accelerated the outflow of the ice sheet, thereby contributing to sea-level rise (Golledge et al., 2015, 2019; DeConto and Pollad, 2016). These phenomena suggest that understanding ocean−ice-sheet interactions in coastal areas of the AIS is important for interpreting contemporary ice-mass loss and for

predicting future ice-sheet behavior. However, the length of the satellite and oceanographic observational records (several decades) is considered to be insufficient to capture the large-scale and potentially non-linear (abrupt) response of the AIS to global climatic change, meaning that understanding of the mechanisms and drivers about the process enacting of abrupt deglaciation is limited (Bentley, 2010).

An effective approach to understanding the mechanisms and drivers of large-scale and abrupt deglaciation is reconstruction of ice-sheet history based on investigation of glacial landforms and determination of the timing of the retreat using surface exposure dating (SED) along transects (both vertical and horizontal) in ice-free areas, especially for the period since the Last Glacial Maximum (LGM) (e.g., Stone et al., 2003; Bentley et al., 2017). Although several reconstructions of ice-sheet history have been made for the western Indian Ocean sector (Dronning Maud Land and Enderby Land), East Antarctica (e.g., Nishiizumi et al., 1991; Moriwaki et al., 1992; Altmaier et al., 2010; Yamane et al., 2011; Suganuma et al., 2014; White and Fink, 2014), the timing and magnitude of ice-sheet change there since the LGM remain unclear. As deglaciation of the AIS since the LGM is thought to have been spatially and temporally variable (Mackintosh et al., 2014; Small et al., 2019), regional geological constraints (e.g., vertical and/or horizontal transect chronology) on change in the AIS in various parts of Antarctica are needed, especially in coastal areas, to understand ocean−ice-sheet interactions and their impact on ice-sheet dynamics.

Knowledge of the long-term history of the AIS is also required to estimate the current ice-mass balance based on satellite gravity measurements, as long-term glacial isostatic adjustment (GIA) has a significant effect on geodetic signals (Whitehouse et al., 2019). Owing to the lack of sufficient geological constraints on vertical and/or horizontal transect chronology in East Antarctica, current GIA model predictions in the western Indian Ocean sector of the Antarctic continent show marked variation in the amplitude of isostatic uplift rates and their spatial distribution, ranging from 1 to 5 mm yr^{-1} (Ivins and James, 2005; Whitehouse et al., 2012; Briggs et al., 2014; Peltier et al., 2016). Moreover, the current crustal deformation rates in the Weddell Sea region observed by the Global Navigation Satellite System (GNSS) shows clear discrepancies from the GIA models, which is thought to due to assumption of the monotonic melting of the AIS during the mid-to-late Holocene used in these models (Bradley et al., 2015). As a result of the variation in the GIA models and their uncertainty, the modeled ice-sheet retreat history also contains significant uncertainty, which is directly linked to uncertainties in current estimates of the mass balance of the AIS and its contribution to contemporary sea-level rise. Therefore, detailed reconstructions of the history of the AIS since the LGM, especially in Dronning Maud Land in the western Indian Ocean sector, are urgently needed.

The Soya Coast is located on the eastern side of Droning Maud Land and faces the Cosmonauts Sea across Lützow-Holm Bay (Fig. 1a). This geographic configuration is considered suitable for investigating the potential impact of ocean−ice interactions on the deglaciation of the AIS. On the basis of faunal analysis of fossil foraminifera of marine sedimentary records, Igarashi et al. (2001) reported that mCDW intrusion into Lützow-Holm Bay during the Holocene might have contributed to ice-sheet retreat along the Soya Coast. However, the relationship between mCDW and ice-sheet retreat remains unclear because neither the timing nor magnitude of the retreat has been well constrained. Although four surface exposure ages have been obtained from one of the ice-free areas (Skarvsnes) of the Soya Coast (Yamane et al., 2011), the detailed ice-sheet history has not yet been reconstructed, which limits evaluation of the potential impact of ocean−ice interactions

on deglaciation of the AIS.

This study aimed to ascertain changes in the altitude and spatial extent of the AIS since the LGM on the southern Soya Coast, Dronning Maud Land, on the basis of field geomorphological observations and newly determined surface exposure ages. Using these data, we provide evidence for an episode of abrupt thinning and retreat of the AIS in this region over a short time interval between the Early (11.2−8.2 ka) and Mid (8.2−4.2 ka) Holocene, and discuss the possible mechanisms and drivers of the abrupt deglaciation.

2. Previous work and ice-sheet configuration along the Soya Coast

The Soya Coast is a north−south-oriented ice-free coastal area extending for ~120 km along the eastern shore of Lützow-Holm Bay, Dronning Maud Land, East Antarctica (Fig. 1a). The ice-free areas are composed mostly of crystalline bedrock of gneiss (e.g., Ishikawa et al., 1977; Nakai et al., 1979; Osanai et al., 2004) and are separated by outlet glaciers, including Langhovde, Honnör, Telen, Skallen, and Vågs glaciers (Fig. 1b).

Raised beach sediments are widely distributed at ~20 m above sea level along the Soya Coast, and ^{14}C ages of marine fossils (shells, polychaete tubes, and foraminifera) in these sediments have been reported (Yoshida, 1983; Hayashi and Yoshida, 1994; Maemoku et al., 1997; Miura et al., 1998a, 1998b, and 1998c). Miura et al. (1998a) presented detailed descriptions of sedimentary structures and ^{14}C dates of in situ fossil shells of the fragile bivalve *Laternula elliptica* found in the sediments. ^{14}C ages obtained from the northern Soya Coast can be clearly divided into two age groups: Holocene (ca. 5−4 ka) and pre-35 ka. In contrast, ^{14}C ages from the southern Soya Coast show only Holocene ages (7−3 ka) (Miura et al., 1998a, 1998c; Takada et al., 2003). Miura et al. (1998a) thus concluded that the northern Soya Coast had not been covered by the East Antarctic Ice Sheet (EAIS) during the LGM, as the existence of pre-35 ka in situ fossil shells suggests that the ice sheet did not overlie the area after their burial. The limited extent of the EAIS during the LGM is considered to be consistent with the geomorphological features between the northern and southern Soya Coast. Bedrock is deeply weathered along the northern Soya Coast, whereas in the southern part, bedrock is unweathered, and ice erosion micro-topographic features, such as glacial striations, are clearly observed (Miura et al., 1998b). An alternative interpretation of these various characteristics, as proposed by Verleyen et al. (2017), is that the LGM ice sheet was nonerosive or cold based and was slow-moving over the Soya Coast area, which also accounts for the in situ fossil shells preserved in the raised beach sediments. In either case, the EAIS is thought to have overlain the southern Soya Coast during the LGM and then to have retreated during the Holocene (Miura et al., 1998a). This is consistent with the results of SED (10−6 ka) from the southern Soya Coast (Yamane et al., 2011).

In Lützow-Holm Bay, several conspicuous and deep submarine valleys exist immediately off the present ice streams along the Soya Coast (Moriwaki and Yoshida, 1983) (Fig. 1a). Igarashi et al. (2001) reported calcareous foraminifera, including *Bulimina aculeata*, from two sediment cores (81−110402 and 81−110901) from the submarine valleys (Fig. 1b), indicating intrusion of mCDW into the valleys. Although the chronology of the cores was poorly constrained owing to the limited number of ^{14}C ages for bulk organic carbon, calcareous foraminifera were observed to have a continuous distribution throughout the cores, indicating intrusion of warm, nutrient-rich, $CaCO_3$-saturated water; i.e., intrusion of mCDW from the offshore area via submarine valleys into the
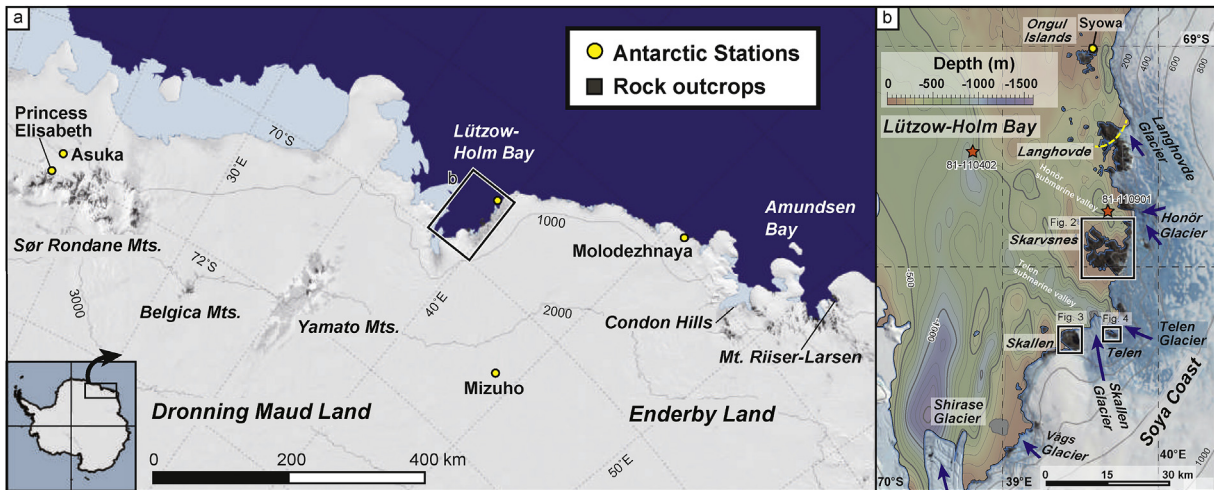
Fig. 1. (a) Overview map of Antarctica, showing the study area in the Indian Ocean sector (Dronning Maud Land and Enderby Land), based on Quantarctica GIS package compiled by the Norwegian Polar Institute (http://www.quantarctica.org/). (b) Satellite image of the Soya Coast. Blue arrows indicate the flow directions of major ice streams in this area. Areas north of the dashed yellow line were probably not covered by the EAIS during the LGM (Miura et al., 1998a). Orange stars show marine sediment sampling sites that include *Bulimina aculeate* calcareous foraminifera. Bathymetry is from the regional bathymetric chart of Moriwaki and Yoshida (1983). (For interpretation of the references to colour in this figure legend, the reader is referred to the Web version of this article.)

southeastern coast of Lützow-Holm Bay during the Holocene (Igarashi et al., 2001).

3. Study area

Geomorphological observations and rock sampling for SED were carried out at three localities along the southern Soya Coast: Skarvsnes, Skallen, and Telen (Fig. 1b). The fieldwork focused on establishing transects and the distances of features from the current ice-sheet margin to reconstruct temporal variations in the altitude and spatial extent of the EAIS along the Soya Coast.

3.1. Skarvsnes

Skarvsnes is the largest ice-free area (63 km^2) along the Soya Coast (Yoshida, 1983), protruding from the ice sheet by ~12 km, and the maximum elevation in this area is 400 m a.s.l. (Skjegget) (Fig. 2). The submarine valleys of Honnör and Telen flank Skarvsnes (Fig. 1b). The geomorphology of this area is characterized by low hills, shallow linear depressions controlled by geological structure, and numerous lakes (Yoshida, 1983). Raised beaches containing marine fossils (shells, polychaete tubes, and foraminifera) are well developed in many places along the present shoreline and can be found up to 23 m above sea level (Hayashi and Yoshida, 1994).

Marine fossil ^{14}C dates obtained using accelerator mass spectrometry (AMS) range from 8860 to 2000 yr BP (Miura et al., 1998c and reference therein). On the basis of the oldest ^{14}C date (7170 yr BP) of in situ *Laternula elliptica*, Skarvsnes is estimated to have become ice free by at least ca. 7 ka (Miura et al., 1998a). Similarly, ^{14}C dates of lake sediment core bottoms obtained from Skarvsnes range from 7650 to 3050 yr BP (Takano et al., 2012; Verleyen et al., 2017). Assuming that ages of lake sediment core bottoms record the timing of ice-sheet retreat (e.g., Hodgson et al., 2001; Verleyen et al., 2004), Verleyen et al. (2017) estimated that Skarvsnes has been ice free from at least the beginning of the Mid-Holocene (around 7650 yr BP), consistent with the oldest ^{14}C dates of in situ *Laternula elliptica* (Miura et al., 1998a).

Yamane et al. (2011) determined the timing of ice-sheet retreat based on SED of four erratic rocks located close to the present ice-sheet margin at Skarvsnes (within ~5 km) (Fig. 2). Although

temporal variations in the thickness and extent of the ice sheet were not well constrained by that study, Skarvsnes is thought to have been covered by a >360-m-thick ice sheet during the LGM and became ice-free between ca. 10 and 6 ka (Yamane et al., 2011).

3.2. Skallen

Skallen is the third-largest ice-free area (14.4 km^2) along the Soya Coast (Miura et al., 1998c), protruding northwestward from the ice sheet and attaining a maximum height of 186 m a.s.l. (Fig. 3). This ice-free area is close to Skallen Glacier and the Telen submarine valley (Fig. 1b). Skallen has a gently undulating surface with two main geomorphological elements that are separated by a wide east−west-trending valley and Lake Skallen Ô-Ike: a northern part with a maximum elevation of 186 m a.s.l. and a southern part with a maximum elevation of 142 m a.s.l. Glacially eroded surfaces are better preserved than those of Skarvsnes and include striations, grooves, and small erosional marks (Sawagaki and Hirakawa, 1997). Raised beaches are found along the eastern coast and around Lake Skallen Ô-Ike below ~15 m a.s.l. (Yoshida, 1983). Along the strandline of northeastern Skallen, unconsolidated sediments are distributed as several ridges that attain heights of up to 20−40 m (Hayashi and Yoshida, 1994). Hayashi and Yoshida (1994) concluded that these ridges are lateral moraines formed by Skallen Glacier, given their composition of mainly gravel and boulders and the lack of marine sedimentological features.

Lake Magoke-Ike is a glacier lake located on the southeastern side of Skallen (Fig. 3). Around Lake Magoke-Ike, gray silty-clay and sand sediments with abundant shell fragments are found (Igarashi et al., 1995; Maemoku et al., 2008). Two ^{14}C ages (3180 yr BP and 3790 yr BP) have been reported from fossil shell fragments (*Laternula elliptica*) in the sediments (Igarashi et al., 1995). This sedimentary setting and the ^{14}C ages of the fossil shells can be explained by a re-advance of the EAIS during the Late Holocene (Maemoku et al., 2008).

^{14}C ages from fragmented marine fossils obtained from Skallen range from 7810 to 3180 yr BP (Igarashi et al., 1995). In addition, bottom sediment of Lake Skallen Ô-Ike has yielded a ^{14}C age of 7219 ± 41 yr BP (Takano et al., 2012). The ages suggest that the initiation of retreat of the EAIS occurred at least from the beginning
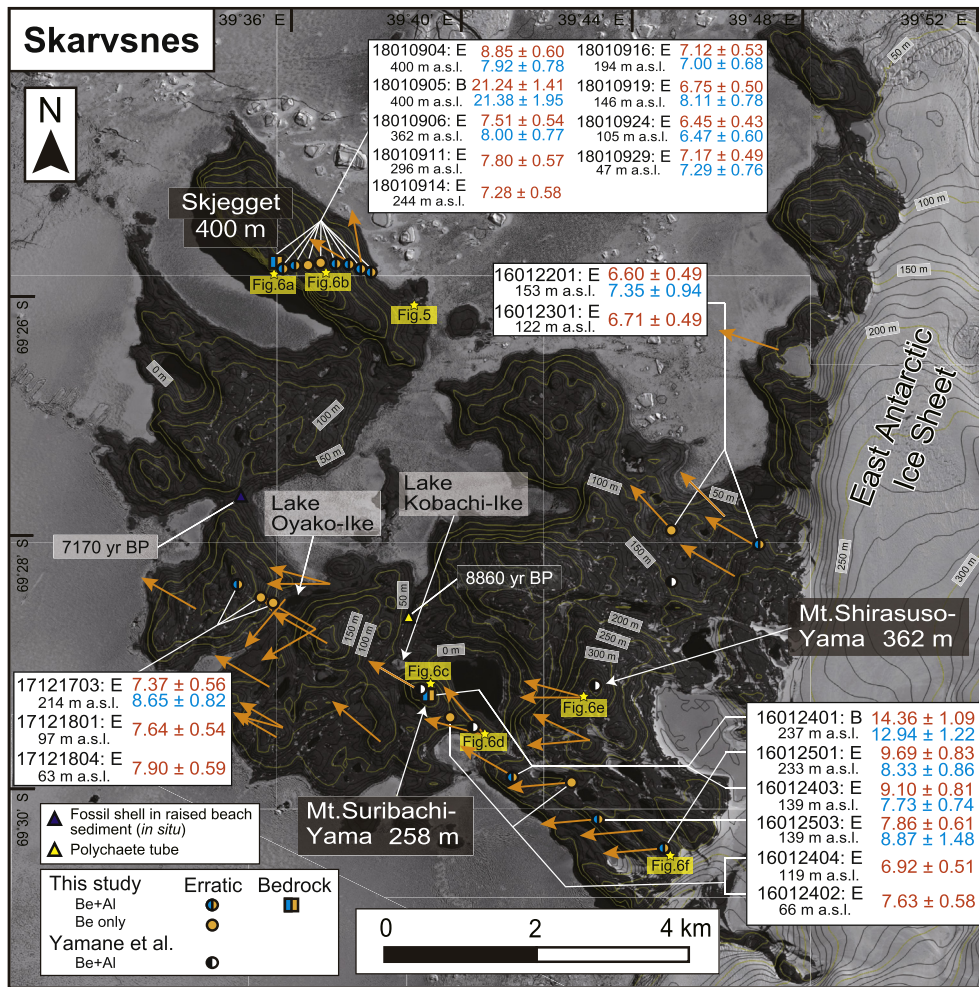
Fig. 2. Satellite image of Skarvsnes derived from Panchromatic Remote-sensing Instrument for Stereo Mapping mounted on the Advanced Land Observing Satellite (ALOS/PRISM). Yellow stars show each location of Figs. 5 and 6. Orange arrows show the orientation of striations identified in this study. Sample sites and ages for surface exposure dating are also shown, with orange and blue symbols/numbers indicating Be and Al SED sites/ages, respectively. Contours are 10 m (black) and 50 m (yellow) intervals, and are derived from the TanDEM-X 90 m Digital Elevation Model (Wessel et al., 2018). (For interpretation of the references to colour in this figure legend, the reader is referred to the Web version of this article.)

of the Mid-Holocene (ca. 7 ka) at Skallen.

3.3. Telen

Telen is a small ice-free area located to the east of Skallen and has a maximum elevation of 106 m a.s.l. (Fig. 4). Unlike Skarvsnes and Skallen, which protrude from the ice sheet as peninsulas, Telen is surrounded by Skallen and Telen glaciers and is located in the upper (terrestrial) part of the Telen submarine valley. Skallen Glacier flows to the NNW on the southern side of Telen, and Telen Glacier flows to the NW on the northern side. Several ridges of unconsolidated sediments are clearly developed, relating to the flanking glaciers. No geochronological constraints on ice retreat have been reported from Telen.

4. Methods

4.1. Geomorphological observations and sampling for surface exposure dating

Geomorphological observations were carried out in two austral summer seasons in Antarctica, from December 2015 to February 2016 and from November 2017 to February 2018, through the

support of the Japanese Antarctic Research Expedition (JARE). These observations focused mainly on the degree of weathering of bedrock and on the presence and orientations of glacial striations. The degree of rock weathering has been used in various studies as a proxy for the relative age of ice-sheet retreat (i.e., the length of time that the rock has been exposed) (e.g., Moriwaki et al., 1991, 1994; White et al., 2011; Suganuma et al., 2014; Kanamaru et al., 2018). Glacial striation orientations were measured by magnetic compass and assumed to indicate the direction of paleo ice flow. Magnetic north in the study area was corrected to true north using the 50° west declination of the IGRF model (Thébault et al., 2015).

A total of 32 samples (29 from glacial erratic rocks and 3 from bedrock surfaces) were obtained for SED from Skarvsnes, Skallen, and Telen (Table 1). Altitudes and locations of the samples were measured using a handheld Global Positioning System device (GPSMAP 62s, GARMIN). We sampled isolated boulders and mostly cobble-sized erratic rocks that appeared to be resting stably on bedrock or moraine to minimize the possibility of post-depositional movement and self-shielding. Most of the erratic rock samples were taken whole from the sampling sites. In contrast, the samples from the bedrock surfaces and some larger erratic rocks were collected by using a handheld electric cutter fitted with a diamond-tipped blade (Suganuma et al., 2012). The advantage of this method
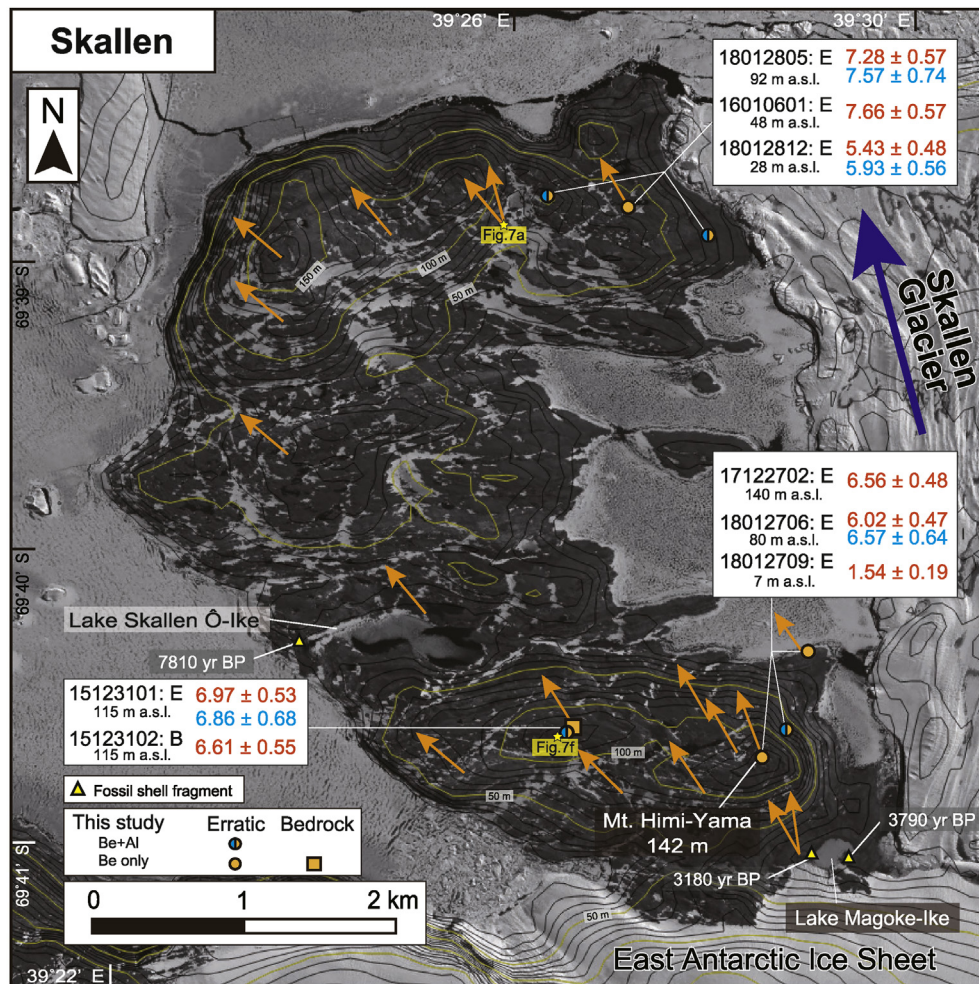
Fig. 3. Satellite image of Skallen derived from ALOS/PRISM. Yellow stars show each location of Fig. 7. The description of the figure is as for Fig. 2. (For interpretation of the references to colour in this figure legend, the reader is referred to the Web version of this article.)

is that the sample can be obtained from a constant depth from the rock surface, thereby minimizing the component of age uncertainty attributable to sample shape heterogeneity. Samples were chosen while avoiding physical weathering, such as sheeting and honey-comb weathering. The topographic shielding effect was measured using a handheld level at the sampling sites and calculated using the CRONUS-Earth online calculators (https://hess.ess.washington.edu/).

4.2. Laboratory analytical techniques

Rock samples were crushed and sieved to 250−500 μm size (with the 250−1000 μm size fraction being used for samples 15123102 and 17122702) to obtain >40 g of clean quartz grains for SED analysis. Elements Be and Al were selectively extracted from the clean quartz grains at the National Institute of Polar Research, Tokyo, Japan, following established methods (Kohl and Nishiizumi, 1992; Bierman et al., 2002). In order to accurate determination of the ^{27}Al concentration in quartz, a part of the sample solution had separated during the experimental processing and used for ^{27}Al measurement by inductively coupled plasma−mass spectrometry (ICP-MS). The weights of the samples and carriers listed in Table 2 show residual weights for AMS measurement after aliquoting for ^{27}Al measurement. $^{10}Be/^9Be$ and $^{26}Al/^{27}Al$ ratios were measured using 40−60 g of clean quartz grains at the Purdue Rare Isotope

Measurement (PRIME) Laboratory, Purdue University, US (Table 2). Measurements were normalized to the 07KNSTD Be standard material with nominal $^{10}Be/^9Be = 2.851 \times 10^{-12}$ (Nishiizumi et al., 2007) and to the KNSTD Al standard material with nominal $^{26}Al/^{27}Al = 1.818 \times 10^{-12}$ (Nishiizumi, 2004). Procedural blanks (n = 5) and samples were both spiked with ~0.5 mg ^9Be carrier (Be carrier, 347.5 μg Be/g). Blanks were spiked with ~1.5 mg ^{27}Al carrier (Al carrier, 728 ppm), and samples were spiked with ca. 1.0 mg ^{27}Al carrier with the value depending on the native Al content of the sample. Blanks ranged from 3×10^{-15} to 30×10^{-15} [$^{10}Be/^9Be$] and 1×10^{-15} to 12×10^{-15} [$^{26}Al/^{27}Al$]. Concentrations reported in Table 2 involved subtraction of background ^{10}Be and ^{26}Al atoms measured in one procedural blank (Tables 2 and 3). Uncertainties include a propagated AMS sample/lab-blank uncertainty, and a 3% uncertainty reflecting stable ^{27}Al measurement by ICP−MS. Unfortunately, ^{26}Al determinations for some samples were unable to be properly measured by AMS owing to interference by high concentrations of ^{26}Mg.

4.3. Exposure age calculations

Surface exposure ages were calculated using the CRONUS-Earth V3 (http://hess.ess.washington.edu/math/v3/v3_age_in.html) on-line calculators (Balco et al., 2008). Exposure ages were calculated using a ^{10}Be half-life of 1.387 Ma (Chmeleff et al., 2010; Korschinek
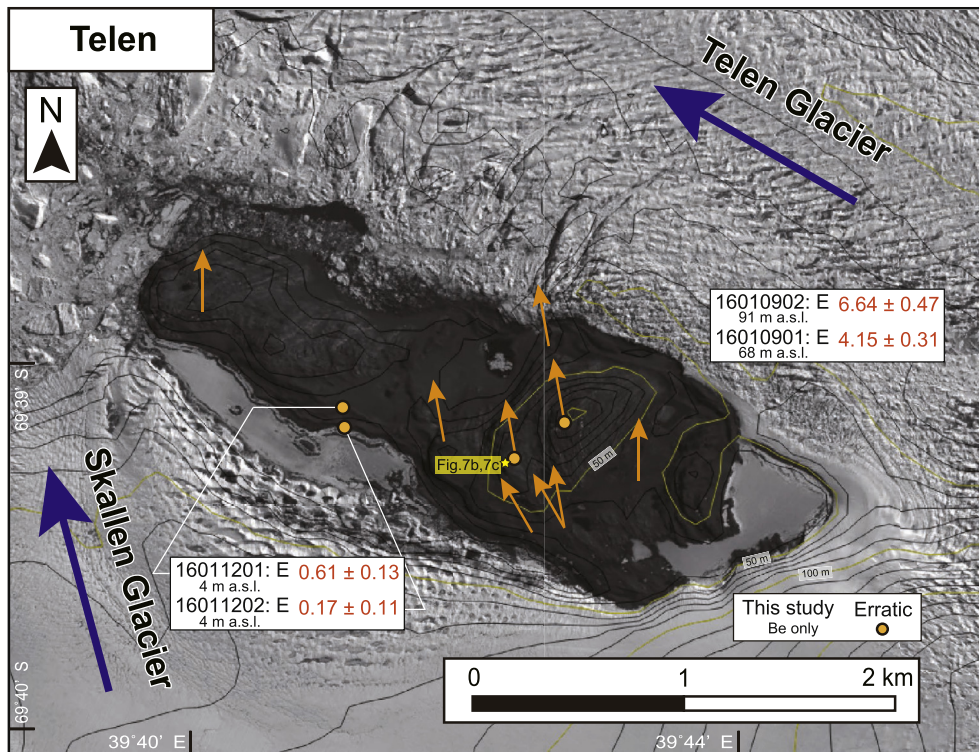
Fig. 4. Satellite image of Telen derived from ALOS/PRISM. Yellow stars show each location of Fig. 7. The description of the figure is as for Fig. 2. (For interpretation of the references to colour in this figure legend, the reader is referred to the Web version of this article.)

et al., 2010) and an [26]Al half-life of 0.705 Ma (Nishiizumi, 2004) with the CRONUS-Earth production rates (Borchers et al., 2016) and employing the Lal−Sato−Dunai nuclide-specific (LSDn) scaling scheme (Lifton et al., 2014). Rock density was assumed to be 2.7 g cm^{-3} for quartz-bearing erratic rock and bedrock samples. Multiple-isotope ([10]Be and [26]Al) cosmogenic nuclide data are useful for understanding either single-exposure (simple-exposure) or complex-exposure and burial ice-sheet histories (Jones et al., 2017). In this study, [10]Be-based exposure ages were used as the main basis for interpretation and discussion because the production rate of [10]Be is better constrained than that of [26]Al (Gosse and Phillips, 2001). [26]Al-based exposure ages were used to check their correspondence to [10]Be-based exposure ages (within error ranges), considering the possible problems relating to sample selection and collection, and to validate the experimental accuracy of quantification of nuclides. All ages are apparent exposure ages, which means that an inherited component might be included. In addition, the age determinations assume that the samples did not undergo self-shielding by rolling and were unweathered, which was handled by collecting erratic rocks resting stably on bedrock or moraine with little surface weathering. We made no attempt to account for the minor variation in production rate caused by GIA, as any influence on age by elevation changes associated with GIA of the Soya Coast is very limited (up to 1%−2%) (Jones et al., 2019). The SED results published for Skarvsnes (Yamane et al., 2011) were recalculated using the same procedure as described above. Uncertainties in SED in this study derive from external errors, including scaling and production-rate uncertainties, as well as internal uncertainties (concentration uncertainties based on laboratory/AMS measurements).

5. Results

5.1. Geomorphology

5.1.1. Skarvsnes

Skjegget (400 m a.s.l.) is an asymmetrical peak located in the northwestern part of Skarvsnes (Figs. 2 and 5). This peak is cliffed on its southwest side, but the northeast slope is relatively gentle. Differences in the degree of weathering of bedrock surfaces on Skjegget are clearly observed with elevation change. The bedrock at and near the summit is strongly honeycomb weathered (Fig. 6a), similar to that of the northern Soya Coast, where fossil shells older than the LGM (pre-35 ka ages) have been reported (Maemoku et al., 1997; Miura et al., 1998b). In contrast, elevations of 250−300 m a.s.l. are characterized by less intense physical weathering, with honeycomb weathering becoming inconspicuous, and smooth surfaces dominating (Fig. 6b).

Mt. Suribachi-Yama (258 m a.s.l.) is a large rocky hill measuring 1500 m long and 300 m high in the central part of Skarvsnes. This hill is interpreted as a particularly large roche moutonnée (Sawagaki and Hirakawa, 1997, 2002b) (Fig. 2). In contrast to the highly weathered bedrock surface at the top of Skjegget (400 m a.s.l.), the bedrock surface on Mt. Suribachi-Yama is relatively unweathered and shows striations (oriented N60°W) (Fig. 6c). Cross-cut striations (N100°W overlapping N50°W) are clearly seen at lower altitudes on the southeastern (ice sheet) side of Mt. Suribachi-Yama (Fig. 6d). The cross-cut striations suggest that the direction of ice-sheet flow changed from N50°W to N100°W.

Mt. Shirasuso-Yama (362 m) is the second-highest peak, is located in the eastern part of Skarvsnes, and is closer to the present ice-sheet margin than are Skjegget and Mt. Suribachi-Yama (Fig. 2). Bedrock weathering of Mt. Shirasuso-Yama is characterized by relatively weak physical weathering from the base to near the

Table 1
Sample information for surface exposure dating.

Sample Name	Latitude (°S)[a]	Longitude (°E)[a]	Altitude (m)[a]	Type	Thickness(cm)	Shielding factor[b]	Sample size (m)
Skarvsnes							
16012401	69.4879	39.6509	237	Bedrock	2.5	0.987	−
16012403	69.4992	39.6836	139	Erratic	2.3	1.000	1.7 × 1.1 × 1.0
16012501	69.5085	39.7439	233	Erratic	2.6	0.982	1.1 × 0.8 × 0.8
16012402	69.4914	39.6617	66	Erratic	2.2	0.987	2.5 × 2.0 × 1.7
16012404	69.4995	39.7092	119	Erratic	2.7	0.996	0.8 × 0.7 × 0.5
16012503	69.4992	39.6836	139	Erratic	2.6	0.998	0.8 × 0.7 × 0.4
16012201	69.4658	39.7831	153	Erratic	2.5	0.999	1.3 × 1.0 × 1.0
16012301	69.4642	39.7464	122	Erratic	2.3	0.997	1.0 × 0.7 × 0.5
18010904	69.4303	39.5944	400	Erratic	5.0	0.994	cobble
18010905	69.4303	39.5944	400	Bedrock	2.5	0.998	−
18010911	69.4302	39.6041	296	Erratic	5.0	0.990	cobble
18010916	69.4288	39.6087	194	Erratic	4.5	0.978	cobble
18010924	69.4301	39.6196	105	Erratic	4.0	0.990	cobble
18010929	69.4298	39.6266	47	Erratic	4.5	0.994	cobble
17121703	69.4729	39.5796	214	Erratic	2.5	0.998	cobble
18010906	69.4300	39.5987	362	Erratic	4.0	0.996	cobble
18010914	69.4297	39.6061	244	Erratic	3.5	0.994	cobble
18010919	69.4296	39.6151	146	Erratic	3.0	0.989	cobble
17121801	69.4751	39.5879	97	Erratic	4.0	0.991	cobble
17121804	69.4755	39.5905	63	Erratic	4.0	0.976	cobble
Skallen							
15123101	60.6775	39.4431	115	Erratic	2.2	1.000	−
15123102	60.6775	39.4431	115	Bedrock	2.5	1.000	−
16010601	69.6464	39.4525	48	Erratic	2.4	1.000	−
17122702	69.6786	39.4765	140	Erratic	4.5	0.989	cobble
18012706	69.6775	39.4818	80	Erratic	4.0	0.995	cobble
18012805	69.6463	39.4416	92	Erratic	3.0	0.998	cobble
18012812	69.6483	39.4640	28	Erratic	4.0	0.999	cobble
18012709	69.6728	39.4826	7	Erratic	5.0	0.999	cobble
Telen							
16010901	69.6534	39.7060	68	Erratic	2.0	0.996	−
16010902	69.6515	39.7125	91	Erratic	2.0	1.000	1.3 × 0.9 × 0.8
16011201	69.6509	39.6860	4	Erratic	2.3	0.987	0.8 × 0.7 × 0.3
16011202	69.6517	39.6862	4	Erratic	2.5	0.998	2.1 × 1.3 × 0.8

[a] Latitudes, longitudes, and altitudes were recorded in the field with a Garmin GPSmap 62sc.
[b] The shielding factor was calculated using the online Geometric Shielding Calculator version 1.1 (Balco et al., 2008).

summit of the mountain and by striations at the peak (Fig. 6e). These weathering features differ from those at Skjegget. The orientations of glacial striations change from west (N90°W−100°W) on the southeastern side of Mt. Shirasuso-Yama to northwest at the summit (Fig. 6f). The striae directions of Mt. Suribach-Yama and Mt. Shirasuso-Yama, southern side of Skarvsnes, show a change in flow direction from NW−SE to W−E. This is consistent with the shift from the overlaid ice sheet to valley glaciers, as ice thinned toward the modern-day profile.

5.1.2. Skallen

Glacial striations and smooth surfaces on bedrock are well preserved at Skallen. These features show no variation with altitude or with distance from the present ice-sheet margin, in contrast to those at Skarvsnes. Orientations of the glacial striations change from SE−NW to SSE−NNW from the western to eastern parts of Skallen (Fig. 3). In addition, the SSE−NNW-oriented striations overlap those oriented NW−SE at several sites (Fig. 7a), indicating that the direction of ice-sheet flow changed from NW to NNW, consistent with lowering of the Skallen Glacier as ice thinned toward the modern-day profile.

5.1.3. Telen

Orientations of glacial striations at Telen are mainly N−S (Fig. 7b), consistent with the current flow direction of Skallen Glacier. Striations and small erosional marks (sculpted erosional forms: s-forms) are clearly observed (Fig. 7c). The bedrock weathering features and glacial landforms, including s-forms, are similar to those at Skallen. Several ridges along the strandlines of Skallen

and Telen Glaciers are composed of unconsolidated sediments, such as gravel and boulders, mixed with fine materials and are almost certainly lateral moraines formed by each glacier (Fig. 7d).

5.2. Surface exposure dating

5.2.1. Skarvsnes

We sampled and analyzed 18 erratic rocks and 2 bedrock surfaces through an elevation range of 47−400 m a.s.l. at Skarvsnes (Figs. 2 and 8a, and b). The surface exposure ages from the erratic rocks lie predominantly in the range 9.7−6.5 ka and show a progressive younging with decreasing elevation (Figs. 5 and 8a, and b). Bedrock surfaces yielded older ages, namely, 21.2 ka and 14.4 ka (Fig. 2). The bedrock samples were collected from relatively unweathered surfaces at the summit of Skjegget and near the summit of Mt. Suribachi-Yama, with the latter sample being collected from where striations were observed (Fig. 6c).

5.2.2. Skallen

Six erratic rock samples were collected from 7 to 140 m a.s.l. along two transects on the northeastern and southeastern sides of Skallen, facing Skallen Glacier (Figs. 3 and 8c). Rock sample 18012812 was taken from the eastern edge of moraine ridges in northeastern Skallen (Fig. 7e), with the other five samples being taken from on top of bedrock. In addition, erratic rock sample 15123101 and bedrock sample 15123102 were collected from the same location on the western flank of Mt. Himi-Yama to ascertain subglacial conditions, with the bedrock sample being collected from a flat surface with striations (Fig. 7f). Surface exposure ages of

Table 2
Analytical results and information for surface exposure dating.

Sample name	Sample weight (g)[a]	9Be carrier weight (mg)[a]	Al in quartz (μg/g)	Aditional ^{27}Al carrier weight (mg)[a]	^{10}Be/^{9}Be ratio (×10^{-15})[b,c]	^{26}Al/^{27}Al ratio (×10^{-15})[b,d]	^{10}Be conc. (×10^4 atoms/g)[e,f]	^{26}Al conc. (×10^4 atoms/g)[e,g]	^{10}Be age (ka)[h,i]	^{10}Be ± int (ka)[j]	^{10}Be ± ext (ka)[k]	^{26}Al age (ka)[h,i]	^{26}Al ± int (ka)[j]	^{26}Al ± ext (ka)[k]	^{26}Al/^{10}Be ratio	Procedural blank number
Skarvsnes																
16012401	38.52	0.4736	69.69	0	148.5 ± 4.91	400.0 ± 15.1	9.68 ± 0.46	61.99 ± 2.35	14.36	0.68	1.09	12.94	0.49	1.22	6.40 ± 0.39	1
16012403	39.13	0.4747	34.27	1.1019	100.6 ± 3.85	248.5 ± 10.3	5.68 ± 0.38	34.41 ± 1.45	9.10	0.61	0.81	7.73	0.33	0.74	6.06 ± 0.48	1
16012501	38.60	0.4758	161.06	0	109.6 ± 4.12	111.6 ± 6.10	6.51 ± 0.40	39.90 ± 2.20	9.69	0.60	0.83	8.33	0.46	0.86	6.13 ± 0.51	1
16012402	44.63	0.4737	78.04	0	66.90 ± 2.77	–	4.37 ± 0.21	–	7.63	0.36	0.58	–	–	–	–	2
16012404	40.93	0.4415	28.61	0.9575	63.66 ± 2.37	–	4.18 ± 0.18	–	6.92	0.30	0.51	–	–	–	–	2
16012503	44.66	0.4756	84.12	0	74.02 ± 3.36	209.6 ± 29.6	4.90 ± 0.25	39.25 ± 5.56	7.86	0.40	0.61	8.87	1.26	1.48	8.02 ± 1.20	2
16012201	44.05	0.4772	286.51	0	62.45 ± 2.35	51.75 ± 4.79	4.14 ± 0.18	32.99 ± 3.07	6.60	0.29	0.49	7.35	0.69	0.94	7.96 ± 0.82	2
16012301	43.56	0.4753	15.07	1.1226	61.26 ± 2.29	–	4.09 ± 0.18	–	6.71	0.29	0.49	–	–	–	–	2
18010904	58.58	0.4822	148.31	0	129.5 ± 4.20	138.9 ± 6.34	6.81 ± 0.23	44.24 ± 2.06	8.85	0.30	0.60	7.92	0.37	0.78	6.36 ± 0.37	3
18010905	58.79	0.4739	87.24	0	317.5 ± 9.18	648.0 ± 17.0	16.9 ± 0.50	120.6 ± 3.23	21.24	0.63	1.41	21.38	0.58	1.95	7.12 ± 0.28	3
18010911	54.67	0.4791	34.94	0	97.41 ± 4.05	–	5.52 ± 0.24	–	7.80	0.34	0.57	–	–	–	–	3
18010916	60.11	0.3430	89.99	0	122.3 ± 5.24	165.3 ± 6.90	4.50 ± 0.20	31.41 ± 1.35	7.12	0.32	0.53	7.00	0.30	0.68	6.99 ± 0.43	3
18010924	58.54	0.3440	26.56	0	100.5 ± 2.87	488.6 ± 15.9	3.78 ± 0.12	26.98 ± 0.91	6.45	0.20	0.43	6.47	0.22	0.60	7.15 ± 0.33	3
18010929	57.97	0.3431	257.21	0	104.7 ± 3.45	52.61 ± 2.93	3.97 ± 0.14	28.80 ± 1.65	7.17	0.26	0.49	7.29	0.42	0.76	7.26 ± 0.49	3
17121703	60.16	0.3419	194.66	0	136.1 ± 5.83	95.12 ± 3.72	4.93 ± 0.24	41.29 ± 1.62	7.37	0.35	0.56	8.65	0.34	0.82	8.37 ± 0.52	4
18010906	59.48	0.4775	209.59	0	111.3 ± 4.11	93.03 ± 3.91	5.74 ± 0.24	43.48 ± 1.83	7.51	0.31	0.54	8.00	0.34	0.77	7.58 ± 0.45	4
18010914	51.78	0.3406	40.18	0	118.9 ± 5.47	–	4.95 ± 0.26	–	7.28	0.38	0.58	–	–	–	–	4
18010919	60.67	0.3408	133.00	0	116.8 ± 4.54	120.6 ± 4.97	4.15 ± 0.19	35.75 ± 1.48	6.75	0.31	0.50	8.11	0.34	0.78	8.61 ± 0.53	4
17121801	39.55	0.3401	132.17	0	81.84 ± 2.86	–	4.47 ± 0.17	–	7.64	0.30	0.54	–	–	–	–	5
17121804	40.80	0.3406	79.40	0	83.05 ± 3.47	–	4.41 ± 0.20	–	7.90	0.37	0.59	–	–	–	–	5
Skallen																
15123101	43.85	0.4754	69.83	0	62.85 ± 2.65	188.1 ± 8.89	4.17 ± 0.20	29.21 ± 1.39	6.97	0.34	0.53	6.86	0.33	0.68	7.00 ± 0.47	2
15123102	40.42	0.4764	97.43	0	55.28 ± 2.76	–	3.94 ± 0.23	–	6.61	0.38	0.55	–	–	–	–	2
16010601	45.09	0.4763	157.41	0	67.07 ± 2.71	–	4.37 ± 0.20	–	7.66	0.35	0.57	–	–	–	–	2
17122702	56.53	0.2909	52.77	0	122.4 ± 4.29	–	3.96 ± 0.17	–	6.56	0.29	0.48	–	–	–	–	4
18012706	54.67	0.2904	134.51	0	104.6 ± 4.19	89.69 ± 3.99	3.45 ± 0.17	26.88 ± 1.20	6.02	0.30	0.47	6.57	0.30	0.64	7.78 ± 0.52	4
18012805	58.57	0.2895	202.41	0	137.1 ± 6.13	70.64 ± 3.30	4.29 ± 0.22	31.88 ± 1.49	7.28	0.37	0.57	7.57	0.36	0.74	7.43 ± 0.52	4
18012812	58.53	0.2891	69.07	0	97.11 ± 5.34	150.2 ± 5.93	2.96 ± 0.20	23.11 ± 0.92	5.43	0.36	0.48	5.93	0.24	0.56	7.80 ± 0.60	4
18012709	39.57	0.3396	475.78	0	18.91 ± 1.30	–	0.85 ± 0.09	–	1.54	0.16	0.19	–	–	–	–	5
Telen																
16010901	59.88	0.3436	77.46	0	67.00 ± 2.71	–	2.40 ± 0.11	–	4.15	0.19	0.31	–	–	–	–	3
16010902	63.90	0.3429	104.82	0	114.2 ± 4.20	–	3.94 ± 0.15	–	6.64	0.26	0.47	–	–	–	–	3
16011201	49.38	0.3447	78.85	0	11.35 ± 1.25	–	0.34 ± 0.07	–	0.61	0.13	0.13	–	–	–	–	5
16011202	48.30	0.3416	47.32	0	5.89 ± 0.88	–	0.09 ± 0.06	–	0.17	0.11	0.11	–	–	–	–	5

[a] The weights of the samples and carriers show residual weights for AMS after aliquoting for Al measurement.

[b] All nuclide ratio mesured by PRIME lab (Purdue Rare Isotope Measurement Laboratory).

[c] Measurements are normalized to 07KNSTD (Nishiizumi et al., 2007) Be standard material with a nominal ^{10}Be/^{9}Be of 2.851 × 10^{-12}.

[d] Meaasurments are normalized to KNSTD (Nishiizumi, 2004) Al standard material with a nominal ^{26}Al/^{27}Al of 1.818 × 10^{-12}.

[e] Concentrations involved the subtraction of background ^{10}Be and ^{26}Al atoms measured in one procedural blank.

[f] Propagated uncertainties of ^{10}Be include an error in the uncertainties on the AMS measurements of both the samples and the blank.

[g] Propagated uncertainties of ^{26}Al include an error in the uncertainties on the AMS measurements of both the samples and the blank and 3% stable ^{27}Al measurement (ICP-MS) uncertainty.

[h] Ages were calculated with the LSDn scale CRONUS-Earth online calculators, V3 (Balco et al., 2008) (http://hess.ess.washington.edu).

[i] A density of 2.7 g cm^{-3} was used based on the gniss rock of the surface samples and assuming zero erosion.

[j] Int = Internal uncertainties; includes only concentration uncertainties based on lab/AMS measurements.

[k] Ext = External uncertainties; includes internal uncertainties plus scaling and production rate uncertainties.

Table 3
Procedural blank data.

Blank No.	^{9}Be carrier weight (mg)	^{27}Al carrier weight (mg)	^{10}Be/^{9}Be ratio($\times 10^{-15}$)	^{26}Al/^{27}Al ratio($\times 10^{-15}$)	^{10}Be conc.($\times 10^4$ atoms)	^{26}Al conc.(10^4 atoms)
1	0.4759	1.4409	30.5 ± 2.67	2.58 ± 1.87	96.95 ± 8.49	8.29 ± 6.00
2	0.4743	1.4385	5.23 ± 0.83	1.42 ± 2.04	16.58 ± 2.63	4.55 ± 6.56
3	0.4798	1.4517	3.12 ± 0.61	11.9 ± 3.18	10.01 ± 1.96	38.4 ± 10.3
4	0.4767	1.4330	4.43 ± 1.56	0.70 ± 1.00	14.12 ± 4.96	2.23 ± 3.21
5	0.4747	1.4442	2.91 ± 0.56	0.75 ± 1.08	9.24 ± 1.82	2.41 ± 3.47
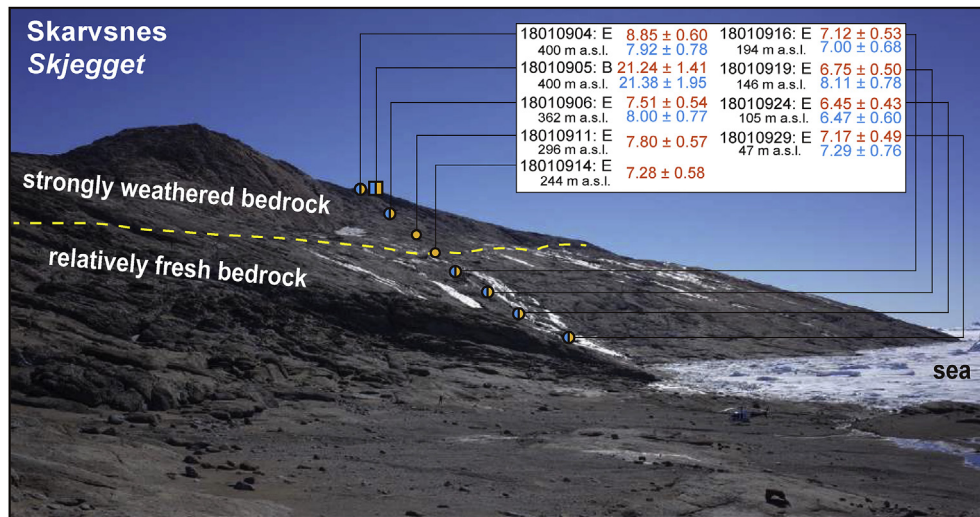
Fig. 5. Overview photograph of Skjegget viewed from the eastside site of Skjegget (Fig. 2), showing sampling sites for surface exposure dating. The dashed yellow line indicates the boundary (at 250 m–300 m a.s.l.) between strongly weathered (above) and relatively fresh (below) bedrock zones, as deduced from field observations. Above the line, bedrock is fractured with honeycomb weathering (Fig. 6a), whereas below the line, bedrock is relatively smooth and largely intact (Fig. 6b). (For interpretation of the references to colour in this figure legend, the reader is referred to the Web version of this article.)

the samples from Skallen range from ca. 8 to ca. 5 ka, except for one young sample (18012709: 1.5 ka). This young rock sample 18012709 is collected from 7 m a.s.l which is the lower than the maximum sea-level height inferred by the raised beach sediments (Yoshida, 1983). However, the relative sea-level at 1.5 ka in Skallen is estimated to be up to ca. 4 m a.s.l. (Verleyen et al., 2017). Thus, the rock sample 18012709 is most likely glacial in origin. The ages of the erratic rock and bedrock samples from western flank of Mt. Himi-Yama are consistent within error (Fig. 3).

5.2.3. Telen

We analyzed four erratic rocks (two samples situated on bedrock and others situated on moraine) sampled from Telen. The sampling elevations cover 4–91 m a.s.l., and exposure ages range from ca. 6.6 to 0.2 ka (Fig. 4). Although the height (4 m a.s.l.) of two samples with young ages (16011201 at 0.6 ka and 16011202 at 0.2 ka) is certainly lower than the maximum sea-level in the area (Yoshida, 1983), they are thought to be glacial in origin. This is because they are from large boulders on the moraine ridge, which are not considered to be ice rafted debris. In addition, the sea-level in this area is thought to become lower than 4 m a.s.l. after 0.6 ka (Verleyen et al., 2017). The ages show a progressive younging with decreasing elevation (Fig. 8d). The two exposure ages (16011201 at 0.6 ka and 16011202 at 0.2 ka) from the erratic rocks of moraine along Skallen Glacier are younger than those of Skarvsnes and Skallen.

6. Discussion

6.1. Interpretation of geomorphic features and exposure ages

Our new surface exposure ages from erratic rocks coupled with field-based geomorphological observations provide clear evidence for an abrupt thinning and retreat of the EAIS along the southern Soya Coast during the Early to Mid-Holocene (ca. 9 to 5 ka). These results also indicate that three ice-free areas (Skarvsnes, Skallen, and Telen) along the Soya Coast were all covered by the EAIS before deglaciation (Fig. 9a and b), most likely during the LGM. However, the exposure ages of bedrock from Skarvsnes (18010905 at 21.2 ka and 16012401 at 14.4 ka) show ages that are older than those of the erratic rocks. These disparities can be explained by inheritance acquired during ice-free periods prior to the LGM.

The bedrock with the oldest exposure age, from the summit of Skjegget (18010905 at 21.2 ka), is characterized by strong honeycomb weathering (Fig. 6a). No striations or glacial polish were observed on the bedrock surface at elevations of >300 m a.s.l. at Skjegget. At this site, the bedrock sample is clearly older than the erratic rock (18010904 at 8.9 ka) in close proximity. Fresh erratic rocks with younger exposure ages on highly weathered bedrock have been explained in terms of being covered by the cold-based AIS (Sugden et al., 2005; Mackintosh et al., 2007; White and Fink, 2014). Because a cold-based ice sheet is less erosive (cf. a warm-based ice sheet) and thus unable to remove the surface of
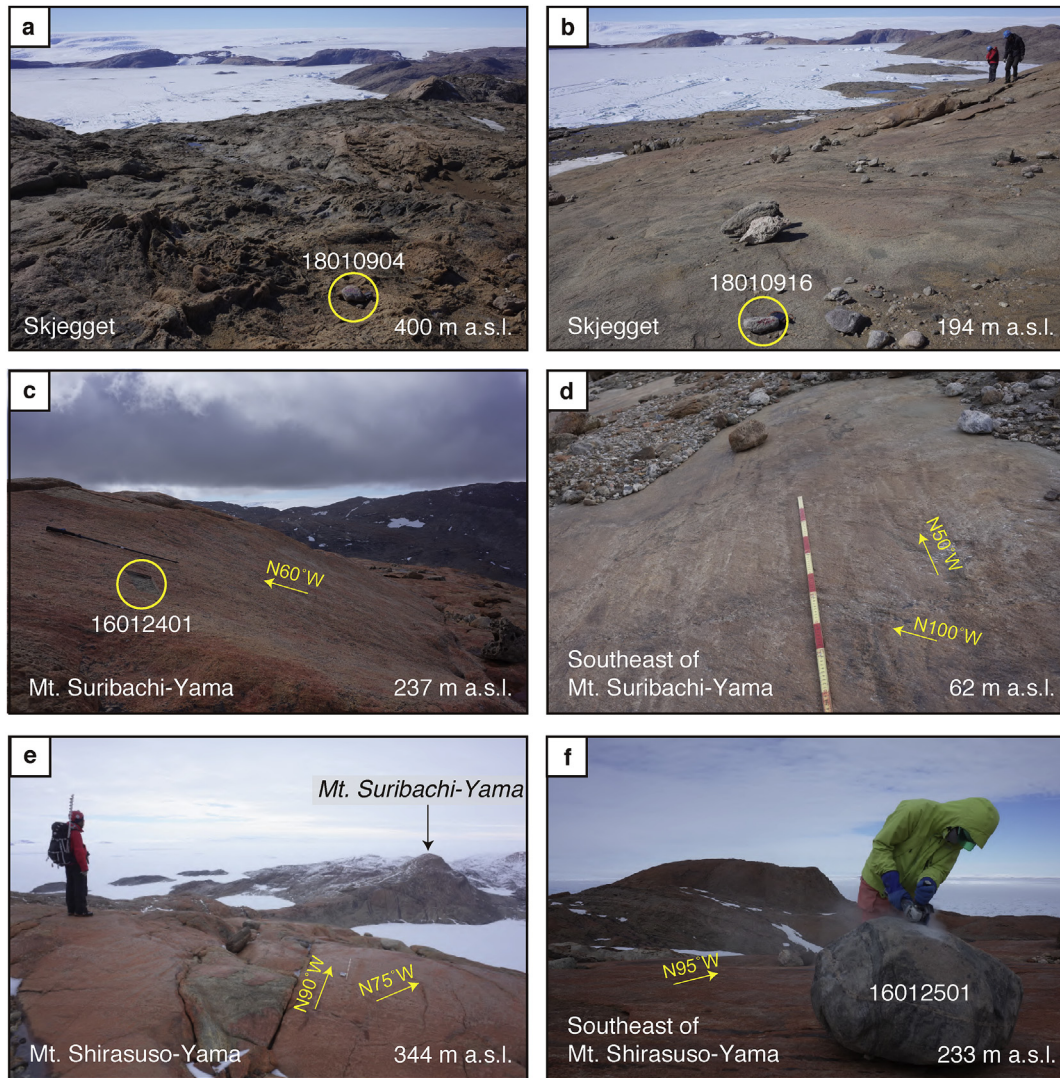
Fig. 6. Glacial geomorphology at Skarvsnes. Localities are shown in Fig. 2. (a) Bedrock at the top of Skjegget, showing intense honeycomb weathering. (b) Sampling site 18010916, at 194 m a.s.l. on Skjegget, showing relatively unweathered and smooth bedrock. (c) Mt. Suribachi-Yama, at an altitude of 237 m a.s.l. (d) Southeastern Mt. Suribachi-Yama, at an altitude of 62 m a.s.l. Cross-cutting striations are clearly observed. (e) Mt. Shirasuso-Yama, at an altitude of 344 m a.s.l. (f) Southern Mt. Shirasuso-Yama, at an altitude of 233 m a.s.l. Striation orientations vary depending on altitude. Yellow circles and arrows show samples for dating and orientations of striations, respectively. (For interpretation of the references to colour in this figure legend, the reader is referred to the Web version of this article.)

bedrock, the weathering state of the bedrock before the last ice advance is thought to have been preserved at Skjegget.

In contrast, the bedrock (16012401 at 6.6 ka) of Mt. Suribachi-Yama is relatively unweathered and partially striated and yielded a slightly younger exposure age (14.4 ka) compared with the summit of Skjegget (Fig. 6c). Geomorphological evidence suggests that subglacial conditions at Mt. Suribachi-Yama were warm based, which would have eroded the bedrock surface, although not sufficiently to remove bedrock down to the ~2 m that is needed to completely reset the inheritance of cosmogenic nuclides (Gosse and Phillips, 2001). Thus, the difference in exposure ages from the bedrock surfaces between Skjegget and Mt. Suribachi-Yama indicates that Skarvsnes was covered not only by cold-based ice sheets during the LGM. The clear transition from weathered to fresh bedrock observed at Skjegget is considered to represent a transition in subglacial conditions from cold- to warm-based ice during the LGM.

Unlike at Skarvsnes, the bedrock (15123102 at 6.6 ka) at Skallen provides an identical exposure age to that of the sampled adjacent erratic rock (15123101 at 7.0 ka). In addition, streamlined bedforms

and s-forms are well preserved around these sampling sites and are thought to have been formed by subglacial meltwater (Sawagaki and Hirakawa, 1997). These features suggest that subglacial erosion at Skallen was more intense than that at Skarvsnes and was significant enough to completely remove any preexisting cosmogenic nuclides in the bedrock. Therefore, subglacial conditions along the southern Soya Coast were not uniform and instead were likely to be highly dependent on ice thickness; i.e., on the relationship between terrain altitude and distance from the ice sheet.

The exposure ages of the sampled erratic rocks allow inferences to be made regarding the timing of thinning and retreat of the EAIS along the Soya Coast. Exposure ages from Skjegget at Skarvsnes show a progressive younging with decreasing elevation, from 8.9 ka at the peak (400 m a.s.l.) to ca. 6.5 ka at ~50–150 m a.s.l. (Fig. 5). In addition, the exposure ages of erratic rocks close to the present ice-sheet margin (e.g., 16012201, 16012503, and 16012501) are also ca. 9–6 ka (Fig. 2). These results suggest that the ice sheet completely covered the Skarvsnes (400 m a.s.l.) prior to ~9 ka and retreated by at least ~10 km over a period of a few thousand years during the
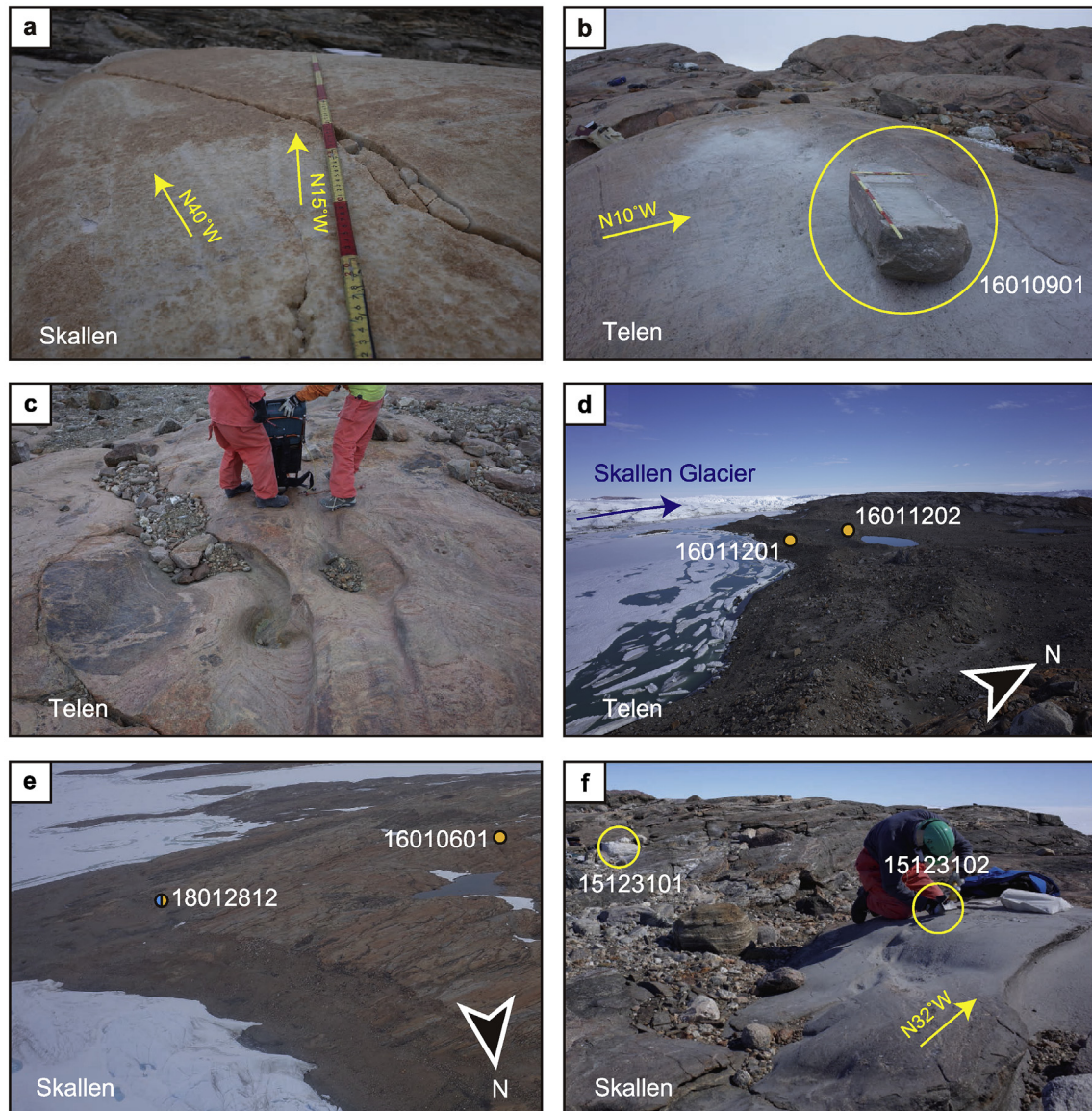
Fig. 7. Glacial geomorphology at Skallen and Telen. Localities are shown in Figs. 2 and 3. (a) N15°W striations cross-cutting N40°W striations at Skallen. (b) Sampling site 16010901 at Telen. (c) Sculpted erosional form at Telen. This form indicates a subglacial meltwater flow event (Sawagaki and Hirakawa, 1997). (d) Lateral moraines flanking Skallen Glacier at Telen. (e) Bird's eye view looking from the northeastern side of Skallen. (f) Bedrock sampling at Skallen, showing unweathered and smooth bedrock. Yellow circles and arrows show samples for dating and orientations of striations, respectively. (For interpretation of the references to colour in this figure legend, the reader is referred to the Web version of this article.)

Early to Mid-Holocene (ca. 9–6 ka). In addition, the ice retreat is thought to be started slightly earlier on the southern side of Skarvsnes, whereas the ice retreat in the northern site might start later, but it was more significant (rapid) than that of the southern side (Fig. 8a and b).

At Skallen, the exposure ages of erratic rocks lie mainly in the range ca. 8–5 ka. The exposure age from the highest site (17122702 at Mt Himi-Yama) is 6.6 ka and is younger than exposure ages (18012805 and 16010601) from the northern part of Skallen, despite lying at lower altitudes than 17122702. As Mt. Himi-Yama is close to the present ice-sheet margin which located ca. 1 km north from the current ice sheet margin (Fig. 3), the slightly younger age can be explained in terms of the terrain having been exposed far from the current ice sheet margin. An exposure age obtained erratic rock from just below the summit at Telen (16010902 at 91 m a.s.l.) indicates that Telen had started to become ice free at 6.6 ka. As the

older exposure age (16010901) was obtained from a higher site (68 m a.s.l.) (Fig. 8d), the ice-sheet thinning rate at Telen is interpreted as having been lower than that at Skarvsnes and Skallen (Fig. 8d). Cross-cutting striations found at Skarvsnes and Skallen (Figs. 6d and 7a) are inferred to have been produced by a change in the direction of ice flow, controlled by the configuration of bedrock topography, during the ice-sheet thinning, which is consistent with the progressive younging of exposure age with decreasing elevation.

The inferred timings of ice-sheet retreat at Skallen (ca. 8–5 ka) and Telen (<ca. 7 ka) are slightly younger than that at Skarvsnes (ca. 9–6 ka). Altitudes of exposure ages from the highest sites at Skallen (140 m a.s.l.) and Telen (91 m a.s.l.) are much lower than those from Skarvsnes (400 m a.s.l.), suggesting that an initiation of the thinning of ice-sheet at Skallen and Telen can be older than the ages obtained from these localities.
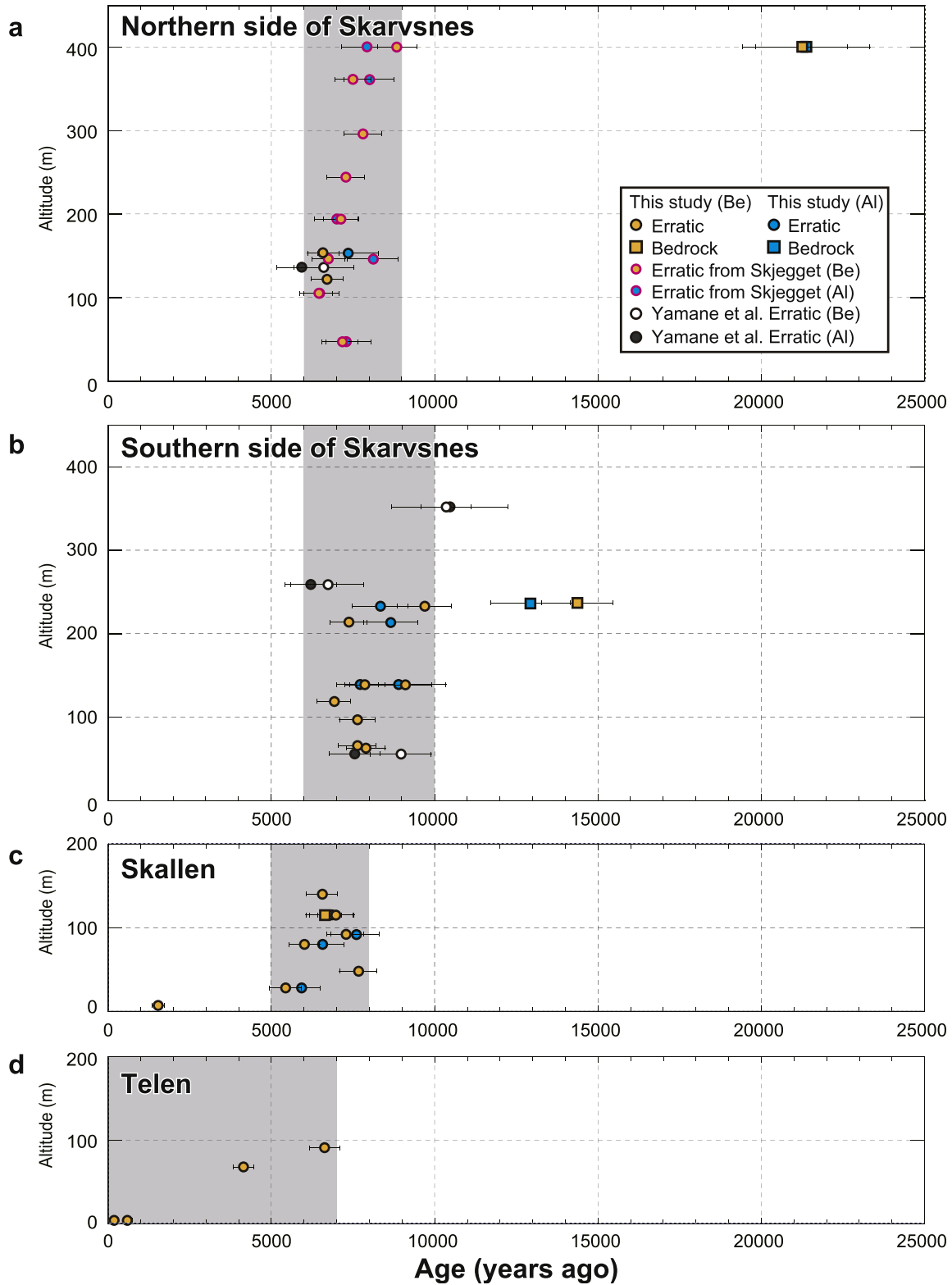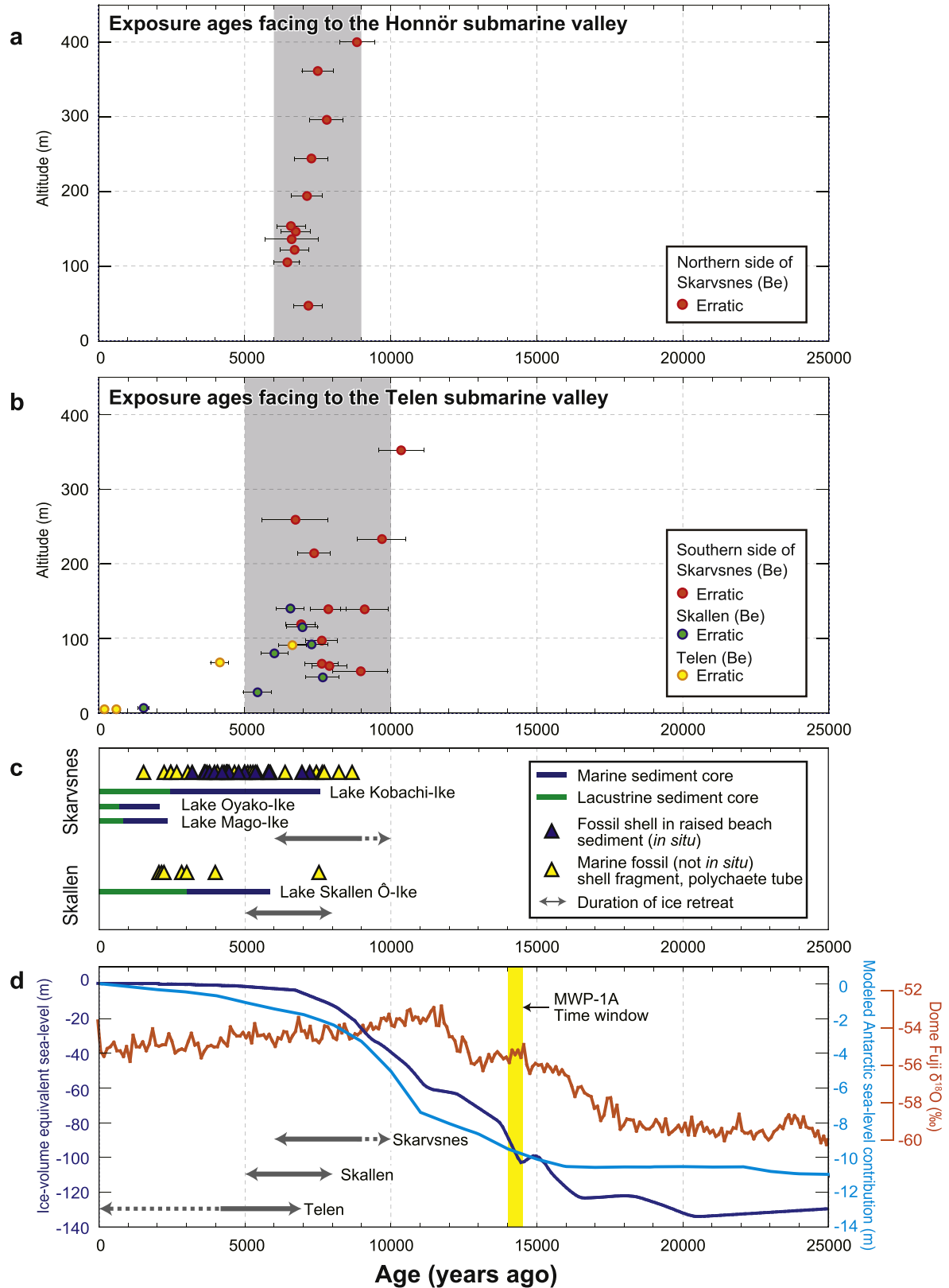
Fig. 8. (a–d) Surface exposure ages plotted against altitude for (a) Northern, (b) southern side of Skarvsnes (with surface exposure ages of erratic rocks from Yamane et al. (2011) also shown), (c) Skallen, and (d) Telen. Surface exposure ages of erratic rocks taken from Skjegget which best evidence for the main phase of thinning recorded in the southern Soya Coast is highlighted. Gray shades show the timings of the ice-sheet retreat in each area. (For interpretation of the references to colour in this figure legend, the reader is referred to the Web version of this article.)

Fig. 9. [10]Be exposure ages of erratic rocks plotted against altitude for (a) facing to the Honnör submarine valley (northern side of Skarvsnes), (b) facing to the Telen submarine valley (southern side of Skarvsnes, Skallen, and Telen) including the exposure ages of Yamane et al. (2011). (c) Calibrated ^{14}C ages (Verleyen et al., 2017) of lake sediments and marine fossils previously published from Skarvsnes and Skallen (Miura et al., 1998c and references therein). (d) δ^{18}O record from Dome Fuji ice core (orange line; Dome Fuji Ice Core Project Members, 2017) plotted alongside ice-volume equivalent global sea-level changes (dark-blue line; Lambeck et al., 2014) and a modeled Antarctic contribution to sea-level change (light-blue line; Briggs et al., 2014) since 25 ka. Dome Fuji Station is located ~1,000 km inland from Syowa Station. The δ^{18}O record obtained from Dome Fuji provide a relative temperature index that represents the surrounding areas in Antarctica. The timing of Meltwater Pulse 1A (MWP-1A) is shown (yellow shading) (Lambeck et al., 2014). The ice-sheet retreat episode of the southern Soya Coast (gray shaded area in panels a and b) does not correspond to any recorded increase in regional atmospheric temperature or significant sea-level rise event such as MWP-1A. (For interpretation of the references to colour in this figure legend, the reader is referred to the Web version of this article.)

These differences in the timing and magnitude of ice retreat are likely controlled the geographical configuration, especially relationship with the submarine valleys. Based on the slight difference in the timing and magnitude of the ice retreat on the southern and north sides of Skarvsnes, the ice retreat in this area is thought to start along the Telen submarine valley, and then propagate to the both sides of the valley (Fig. 9a and b). On the other hand, the ice retreat along the Honnör submarine valley likely starts slightly later, but it was more intensive, probably due to close contact between the mountain flank and the ocean (Figs. 1b and 2). Therefore, we conclude that the EAIS started to thin and retreat at the almost same time along the southern Soya Coast during the Early Holocene (ca. 9 ka), but that propagation was locally variable.

Because the moraine material suggests a change in behavior of glaciers such as re-advance and/or stillstand, surface exposure age of moraine on northern Skallen (18012812) provides evidence for a small re-advance and/or stillstand of the glacier that terminated at ~5.4 ka. Thicker accumulation of glacial debris reaches up to sample 16010901 (~4.2 ka) across the lower flanks of Telen is consistent with this interpretation.

Very young exposure ages were obtained at three sites in Skallen and Telen. The exposure age of 18012709 (ca. 1.5 ka) at Skallen can be explained by a possible re-advance of Skallen Glacier during the Late Holocene. Maemoku et al. (2008) inferred a minor re-advance of the glacier based on geomorphological observations, including shell fragments observed in clayey glacial sediments at Lake Magoke-Ike. On the basis of the ^{14}C age of a shell fragment (ca. 3 ka BP) (Igarashi et al., 1995), we consider that a re-advance of Skallen Glacier occurred after 3 ka. Thus, the exposure age of 18012709 (ca. 1.5 ka) obtained from a site ~1 km north of Lake Magoike-Ike likely represents the timing of retreat of Skallen Glacier after the re-advance event (Fig. 3). The two young exposure ages of erratic rocks (16011201 at 0.6 ka and 16011202 at 0.2 ka) from lateral moraines along Skallen Glacier at Telen are consistent with this interpretation. Thus, a re-advance of Skallen Glacier is thought to have occurred over the present ice-sheet margin during the Late Holocene, probably from ca. 3.0 to 1.5 ka.

The initiation of retreat of the EAIS along the Soya Coast has previously been investigated on the basis of marine fossils and ^{14}C dating of lake sediments from Skarvsnes and Skallen (Miura et al., 1998a, 1998c; Takano et al., 2012; Verleyen et al., 2017) (Fig. 9c). At Skarvsnes, the oldest ^{14}C age of a marine fossil (a polychaete tube) in a raised beach is 8860 yr BP (Miura et al., 1998c), and the oldest bulk ^{14}C age of lake sediments from Lake Kobachi-Ike is 7650 yr BP (Verleyen et al., 2017) (Fig. 9c). At Skallen, the oldest ^{14}C age of a shell fragment (*Laternula elliptica*) in a raised beach is 7810 yr BP (Miura et al., 1998c), and the oldest bulk ^{14}C age of sediments from Lake Skallen Ô-Ike is 6160 yr BP (Takano et al., 2012) (Fig. 9c). These ^{14}C ages from Skarvsnes and Skallen suggest that these areas became ice free during the period ca. 9–6 ka, which is consistent with our geomorphological observations and surface exposure ages.

However, the ^{14}C age from the bottom of a sediment core (total length 153 cm) from Lake Oyako-Ike in Skarvsnes is 3050 yr BP (Takano et al., 2012). This age is younger than exposure ages from Skarvsnes (9–6 ka) and the ^{14}C age of lake sediments from Lake Kobachi-Ike (7650 yr BP). The lithology of the sedimentary core obtained from Lake Oyako-Ike is laminated microbial mat, and no glacial sediments are observed in the lowermost part of the core. The basal parts of lake sediment cores obtained from Antarctic lakes generally comprise glacial sediments (e.g., Hodgson et al., 2001; Watcham et al., 2011), suggesting that sedimentation of lakes in Antarctica should begin with glacial sediments coinciding with the retreat of the AIS. Thus, the ^{14}C age obtained from the

sediment core from Lake Oyako-Ike might not reflect the initiation of sedimentation in the lake (the initiation of ice-sheet retreat). As the ^{14}C age of lake basal sediments indicates only a minimum age of ice-sheet retreat, we suggest that a detailed description of the sedimentary facies, and in particular whether glacial sediments are reached in cores, is needed to ensure correct inferences regarding ice retreat.

Empirical geological evidence of bedrock weathering can also be used to infer ice-sheet thickness along the Soya Coast prior to retreat and thinning of the EAIS. As mentioned, we interpret the transition in bedrock weathering features at Skjegget (Fig. 5) as indicating a change from a warm-to cold-based ice sheet. It is known that poor preservation of strongly weathered bedrock suggests an ice thickness greater than ~300 m (Bentley et al., 2010; Bromley et al., 2010). The highly weathered bedrock with older exposure ages in the upper of Skjegget provides the first-order estimation for the limit on the former ice thickness that overlaid the summit of Skjegget less than ~300 m.

Our interpretation of ice thickness during the LGM along the Soya Coast is consistent with results of numerical modeling studies (Sawagaki and Hirakawa, 2002a; Okuno and Miura, 2013). Two methods (the hydraulic method and GIA modeling) have been used for numerical experiments to estimate ice-sheet thickness during the LGM. Sawagaki and Hirakawa (2002a) conducted a hydraulic numerical experiment to estimate the optimum thickness and shape of an ice sheet that would produce the observed arrangement of streamlined bedforms formed by subglacial meltwater. Those authors found that basal water flow simulated by an ice sheet with a thickness of ~400 m tilted to the west is consistent with the arrangement of streamlined bedforms observed at Skarvsnes. Okuno and Miura (2013) performed relative-sea-level calculations for the Soya Coast and other sites along Antarctic coastal regions by using GIA modeling with different ice and lithosphere parameters. Regardless of lithospheric thickness parameters, those authors found that paleo sea-level observations (Miura et al., 1998a) could not be explained unless an ice sheet of a few hundred meters thick on the Soya Coast had melted since the LGM. Therefore, our estimate of ice thickness during the LGM along the southern Soya Coast (at least 400 m but no more than overlaid ~300 m at Skjegget is consistent with the results of numerical models.

6.2. Timing and magnitude of deglaciation since the LGM in the Indian Ocean sector of the EAIS

Our new exposure ages and geomorphological features indicate that the ice sheet completely covered the highest peak of Skarvsnes (at least 400 m of ice thickness but no more than overlaid ~300 m at summit of Skjegget) and retreated by at least 10 km during the short interval from the Early to Mid-Holocene (ca. 9–5 ka) along the southern Soya Coast. The rate of thinning at Skjegget is estimated to be ca. 0.2 m/yr, which is similar to the other "abrupt thinning" reported at other locations across Antarctica, such as Western Weddle Sea (ca. 1.5 kyr to thin 250 m - i.e. <0.2 m/yr) (Johnson et al., 2019), in the heart of the inner Weddell Sea embayment (ca. 1 kyr to thin 200 m - i.e. 0.2 m/yr) (Hein et al., 2016), and western Marie Byrd Land (ca. 0.9 kyr to thin 330 m - i.e. <0.4 m/yr) (Stone et al., 2003). Such abrupt thinning and retreat of the EAIS have been reported from other parts of the Indian Ocean sector of East Antarctica (White and Fink, 2014). White and Fink (2014) reported exposure ages from erratic rock and bedrock samples from Condon Hills, along the lower part of the Rayner Glacier, in the coastal area of Enderby Land (Fig. 1a). Those authors determined exposure ages of erratic rocks in the upper (560 m a.s.l.) and lower (240 m a.s.l.) parts of Condon Hills of ca. 9 ka and ca. 6 ka, respectively, indicating that >300 m of ice-sheet thinning and

>10 km of retreat occurred during 9—6 ka at Condon Hills.

The thickness of the EAIS that overlaid Condon Hills can also be estimated using geomorphological features. A clear transition in the weathering state of bedrock has been observed within the elevation range of 300—450 m a.s.l. at Condon Hills (White and Fink, 2014). The bedrock above the transition is deeply weathered, whereas that in the lower part of the terrain is relatively unweathered, showing smooth surfaces and striations. In addition, the exposure ages of bedrock in the upper (560 m a.s.l.) and lower (240 m a.s.l.) parts are ca. 103 ka and ca. 26 ka, respectively, and are older than those of adjacent erratic rocks. These geomorphological features and older exposure ages of the bedrock at Condon Hills are similar to those observed at Skarvsnes, which we explain in terms of a transition in subglacial conditions from a warm-to cold-based ice sheet. As ice-sheet thickness controls subglacial conditions (Bentley et al., 2010; Bromley et al., 2010), the thickness of the EAIS that overlaid Condon Hills during the LGM is considered not to have exceeded several hundred meters. Zwartz and Stone (1997) interpreted the LGM ice-sheet thickness at Mt. Riiser-Larsen (Fig. 1a), near Condon Hills, to have been less than 500 m, as no erratic rocks or striated bedrock are found above 500 m a.s.l. there. These SED results and geomorphological features of bedrock from Enderby Land are very similar to our observations for the Soya Coast in Dronning Maud Land (Fig. 1a). Combining the previous results with our new data, we infer that abrupt deglaciation after the LGM occurred essentially simultaneously along the entire coastal area of Dronning Maud Land and Enderby Land during the Early to Mid-Holocene (ca. 9—5 ka).

In contrast to the coastal areas of Dronning Maud Land and Enderby Land, a lower magnitude of ice-sheet thinning in the interior of the EAIS has been inferred from exposure ages and geomorphologic evidence from nunataks in the Sør Rondane Mountains (Moriwaki et al., 1991, 1992; Suganuma et al., 2014) and the Wohlthat Massiv (Altmaier et al., 2010), Dronning Maud Land, East Antarctica. Although the marked ice-sheet thinning since the LGM has been reported in the major ice drainage system such as Lambert Glacier (White et al., 2011) and Rayner Glacier (White and Fink, 2014), the ice-sheet thinning is generally less intensive in the other part of the EAIS interior. Therefore, marked thinning and retreat of the EAIS since the LGM appears to have occurred only in the coastal area and the major ice drainage system in the Indian Ocean sector of East Antarctica.

Detailed reconstructions of the history of the EAIS will contribute to interpret the local crustal deformation observed by the GNSS and calibrate the current GIA models. Ohzono et al. (2006) reported an upward displacement rate of approximately 1 mm/year for 8 years since 1998 at Skarvsnes based on the GNSS observation. Although the effect of the significant snowfall in Dronning Maud Land, observed by the satellite gravity mission in recent years (e.g. Velicogna et al., 2020), is needed to be considered, our detailed reconstruction of the retreat history of the relatively thick EAIS that overlaid the southern Soya Coast since the Early to Mid-Holocene allows us to compare the GNSS data and GIA models in future studies.

6.3. Possible drivers of the abrupt deglaciation since the LGM

To identify the drivers of the abrupt timing and retreat of the EAIS along the southern Soya Coast during ca. 9—5 ka, the scale and potentially non-linear (abrupt) nature of the response of the AIS to global climatic change must be considered, On the basis of ice-core $\delta^{18}O$ records (Dome Fuji Ice Core Project Members., 2017), no clear signal of climate change, such as atmospheric warming, has been identified over this time interval (Fig. 9d). Therefore, changes in atmospheric temperature and/or related snow accumulation rate are not considered drivers for the abrupt thinning and retreat, meaning that an alternative explanation of the melting event is required.

A key consideration for explaining the abrupt deglaciation along the southern Soya Coast is the geographical setting, including the locations of currently ice-free areas (Skarvsnes, Skallen, and Telen) and the bathymetry of the adjacent areas. Deep submarine valleys are incised into Lützow-Holm Bay and extend from the continental shelf to the present ice-sheet margin (Moriwaki and Yoshida, 1983) (Fig. 1b). Skarvsnes and Skallen protrude from the continental ice sheet and face a branch (Telen submarine valley and Honnör submarine valley) of the deep submarine valleys (Fig. 1a). On the basis of marine geological records, Igarashi et al. (2001) suggested that mCDW intruded into the bay via submarine valleys during the Holocene. These valleys are thought to have been formed through selective erosion, controlled by geological structure, by past ice streams (Moriwaki and Yoshida, 1983), including a large outlet glacier that flowed NW—SE along the Telen submarine valley during the last glacial period. Given this geographical configuration, we consider that mCDW intrusion into submarine valleys promoted basal melting and grounding-line migration of the ice sheet along these valleys, causing marine ice-sheet instability. This process likely led to thinning of the EAIS by hundreds of meters along the Soya Coast (Fig. 9a and b and 10). In contrast, Telen is located upstream of the submarine valley and is flanked by glaciers, unlike the other two ice-free areas of Skarvsnes and Skallen (Fig. 1b). We interpret these differences in geographical configuration in terms of marine ice-sheet instability having been relatively minor at Telen, with relatively slow ice-sheet thinning there (Fig. 8c). However, overall, the main determinant of deglaciation along the southern Soya Coast is inferred to be marine ice-sheet instability caused by mCDW intrusion into deep submarine valleys.

Based on this hypothesis, the slight differences in the timing of the initiation of the ice-sheet retreat between the northern and southern sides of Skarvsnes can also be explained by the geographical configuration of this area. The Telen submarine valley, southern side of Skarvsnes, is a large submarine valley with more than 1000 m deep, while the Honnör submarine valley is slightly shallower and smaller (Fig. 1b). This suggests that the Telen submarine valley is potentially more susceptible to mCDW intrusion, which may cause earlier deglaciation in the southern side of Skarvsnes. On the other hand, the Skjegget, northern part of Skarvsnes, is directly facing to the Honnör submarine valley, which may have been more sensitive to the mCDW intrusion and to the ocean—ice-sheet interactions than the southern part of Skarvsnes. Therefore, the initiation of the ice sheet thinning of the northern part of Skarvsnes was slightly later, but the more abrupt thinning was thought to have occurred (Fig. 9a). In addition, the small re-advance and/or stillstand of the Skallen Glacier likely suggest ceasing or weakening of the mCDW intrusion by ~5.4 ka. Overall, our data suggest that the thinning and retreat of the EAIS in the southern part of the Soya Coast have been greatly influenced by the intrusion of the mCDW and ocean—ice-sheet interactions.

In other parts of Antarctica, including Condon Hills, hundreds of meters of ice-sheet thinning over a few thousand years in the Holocene have been reported (Johnson et al., 2014, 2019; Jones et al., 2015; Hein et al., 2016; Spector et al., 2017). A common feature in these studies is that the investigated areas coincide with fast-flowing outlet glaciers. Conversely, deglaciation since the LGM as inferred from nunataks was not significant in Dronning Maud Land, suggesting that the ice-sheet thinning in coastal areas did not propagate into the interior of the EAIS. Therefore, we hypothesize that the difference in ice-sheet thinning since the LGM between coastal areas and the EAIS interior can be explained by different
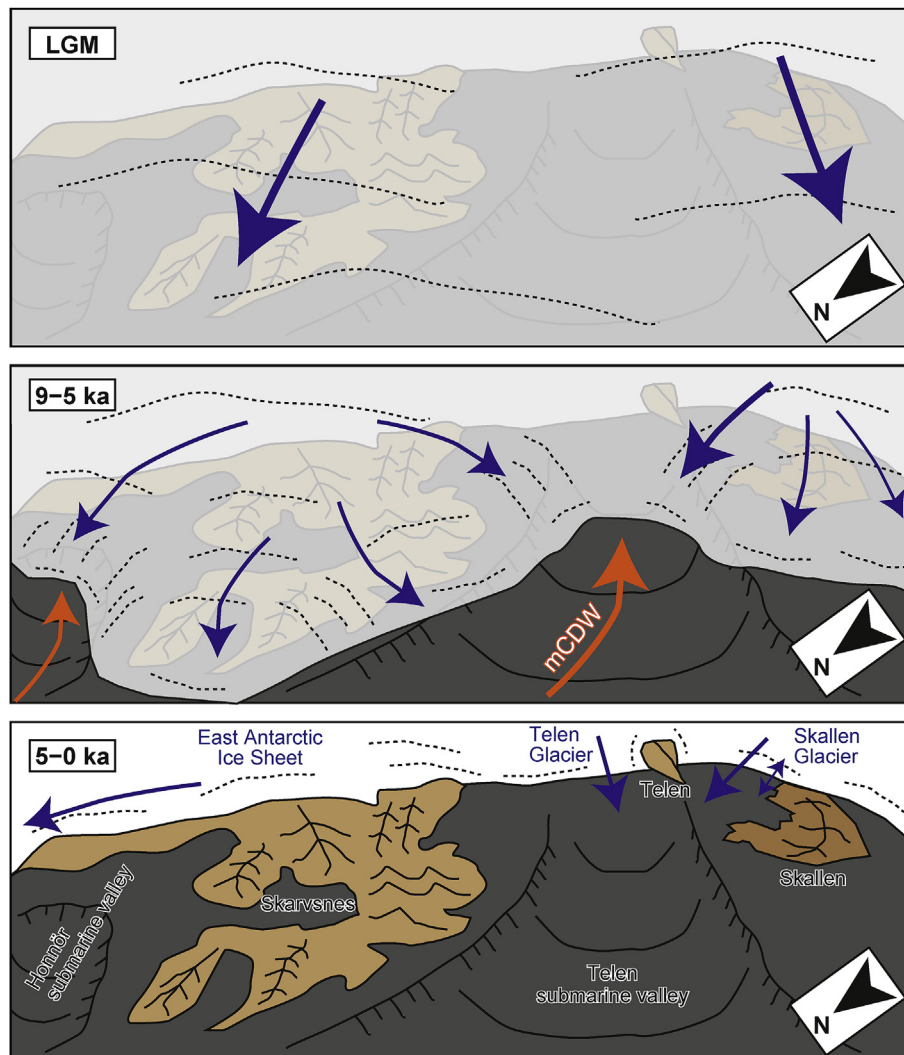
Fig. 10. A conceptual reconstruction of different ice-sheet configurations along the southern Soya Coast (viewed from the northwest). The inferred history of ice-sheet retreat is as follows. The EAIS covered the entire southern Soya Coast during the LGM and had advanced to the northwest, far offshore. The ice sheet abrupt thinning and retreat during the Early—Mid-Holocene (9—5 ka), with flow direction changing as a result of bedrock topographic control. The abrupt thinning and retreat of the EAIS in this area is considered to have been marine ice-sheet instability caused by the intrusion of the modified Circumpolar Deep Water (orange arrows) via deep submarine valley. Subsequently (5—0 ka), the ice sheet retreated beyond the current ice-sheet margin, then slightly re-advanced to the current margin, at least at Skallen. Blue arrows indicate the flow directions of major ice streams in this area. (For interpretation of the references to colour in this figure legend, the reader is referred to the Web version of this article.)

mechanisms of ice-mass change. The loss of ice mass in coastal areas is considered to have been caused predominantly by ice dynamics (fast response) responding to ocean—ice-sheet interactions. In contrast, the change in ice mass in the EAIS interior was likely to have been controlled by water supply from the Southern Ocean (slow response) (Suganuma et al., 2014; Yamane et al., 2015). This hypothesis emphasizes the promotion of ice-sheet thinning at the regional scale by mCDW, extending along the coastal area of the western Indian Ocean sector, but with propagation of the ice-mass loss being restricted by the geographical setting.

The source of Meltwater Pulse 1A (MWP-1A) has been suspected to have in part originated in East Antarctica (Weber et al., 2014; Small et al., 2019). Our exposure ages indicate that the timing of ice-sheet retreat most likely post-dated MWP-1A, implying a minimal contribution by ice-melting along the Soya Coast to MWP-1A (Fig. 9d). However, the extent and thickness of the EAIS in Lützow-Holm Bay during the LGM have not yet been established. Therefore, further studies, especially those based on marine

records, are needed to accurately estimate the contribution of ice mass loss around Lützow-Holm Bay to sea-level rise after the LGM.

Our results suggest that understanding of ocean—ice-sheet interactions to explain ice sheet behavior is important not only for West Antarctica but also for the Indian Ocean sector of East Antarctica. The geographic configuration of Lützow-Holm Bay is highly suitable for investigating these interactions. Therefore, further investigations, including detailed bathymetric observations and marine sediment analysis in addition to SED determinations for the entire Soya Coast should provide valuable information regarding ocean—ice-sheet interactions and abrupt deglaciation since the LGM. In addition, numerical modeling studies using a range of forcings should be applied to test the controls on ice-sheet retreat that caused grounding-line migration, together with a comparison of model results with field observations relating to past ice extent (e.g., Mackintosh et al., 2011; Jones et al., 2015; Whitehouse et al., 2017).

7. Conclusions

We interpreted the ice-retreat history of the southern Soya Coast, Lützow-Holm Bay, East Antarctica, based on new geomorphological observations and transects of surface exposure ages. Our findings allow us to draw the following conclusions.

- The East Antarctic Ice Sheet (EAIS) during the Last Glacial Maximum extended at least 10 km farther than the present ice margin along the southern Soya Coast and had an ice thickness of at least 400 m.
- Surface exposure ages from the southern Soya Coast indicate that abrupt thinning and retreat of the ice sheet occurred during the Early to Mid-Holocene (9−5 ka).
- The ice sheet that overlaid the southern Soya Coast retreated while changing flow direction as controlled by bedrock topography.
- Differences in exposure ages of bedrock-erratic pairs from the same location suggest inheritance in the ages of the bedrock acquired during ice-free periods prior to the last deglaciation. Exposure ages are consistent with geomorphological features, which indicate that the subglacial condition of the ice sheet that overlaid this area was nonerosive cold-based ice and/or warm-based ice which not sufficiently to erode bedrock to completely reset the inheritance of cosmogenic nuclides.
- Although we cannot directly constrain ice thickness during the LGM, evidence from weathering features and inherited age of bedrock at Skjegget (400 m a.s.l.) at Skarvsnes provides the first-order estimation for the limit on the former ice sheet thickness that overlaid the summit of Skjegget less than ~300 m.
- The abrupt ice-sheet thinning and retreat identified along the southern Soya Coast most likely occurred synchronously and with a similar magnitude to that of other Antarctic ice-free areas characterized by fast-flowing outlet glaciers.
- The mechanism of the abrupt thinning and retreat of the EAIS in this area is considered to have been marine ice-sheet instability caused by the intrusion of modified Circumpolar Deep Water via deep submarine valleys.

Authorship contributions

M, Kawamata: Conceptualization, Methodology, Software, Validation, Formal analysis, Investigation, Resources, Data curation, Writing - original draft, Writing - review & editing, Visualization, Project administration, Funding acquisition. Y, Suganuma: Conceptualization, Methodology, Validation, Investigation, Resources, Data curation, Writing - original draft, Writing - review & editing, Visualization, Supervision, Project administration, Funding acquisition. K, Doi: Conceptualization, Investigation, Resources, Writing - original draft, Writing - review & editing, Supervision, Project administration. K, Misawa: Methodology, Validation, Formal analysis, Resources, Writing - review & editing, Supervision. M, Hirabayashi: Methodology, Formal analysis, Resources. A, Hattori: Software, Visualization. T, Sawagaki: Conceptualization, Supervision.

Declaration of competing interest

The authors declare that they have no known competing financial interests or personal relationships that could have appeared to influence the work reported in this paper.

Acknowledgments

Appendix A. Supplementary data

Supplementary data to this article can be found online at https://doi.org/10.1016/j.quascirev.2020.106540.

References

Altmaier, M., Herpers, U., Delisle, G., Merchel, S., Ott, U., 2010. Glaciation history of Queen Maud Land (Antarctica) reconstructed from in-situ produced cosmogenic ^{10}Be, ^{26}Al and ^{21}Ne. Pol. Sci. 4, 42−61.

Balco, G., Stone, J.O., Lifton, N., Dunai, T.J., 2008. A complete and easily accessible means of calculating surface exposure ages or erosion rates from ^{10}Be and ^{26}Al measurements. Quat. Geochronol 3, 174−195.

Bentley, M.J., 2010. The Antarctic palaeo record and its role in improving predictions of future Antarctic Ice Sheet change. J. Quat. Sci. 25, 5−18.

Bentley, M.J., Fogwill, C.J., Brocq, Le, A, M., Hubbard, A.L., Sugden, D.E., Dunai, T.J., Freeman, S.P., 2010. Deglacial history of the west antarctic ice sheet in the Weddell Sea embayment: constraints on past ice volume change. Geology 38, 411−414.

Bentley, M.J., Hein, A.S., Sugden, D.E., Whitehouse, P.L., Shanks, R., Xu, S., Freeman, S.P.H.T., 2017. Deglacial history of the Pensacola Mountains, Antarctica from glacial geomorphology and cosmogenic nuclide surface exposure dating. Quat. Sci. Rev. 158, 58−76.

Bierman, P.R., Caffee, M.W., Davis, P.T., Marsella, K., Pavich, M., Colgan, P., Mickelson, D., Larsen, J., 2002. Rates and timing of earth surface processes from in situ- produced cosmogenic Be-10, Beryllium. Mineral. Petrol. Geochem. 147−205.

Borchers, B., Marrero, S., Balco, G., Caffee, M., Goehring, B., Lifton, N., Nishiizumi, K., Phillips, F., Schaefer, J., Stone, J., 2016. Geological calibration of spallation production rates in the CRONUS- Earth project. Quat. Geochronol. 31, 188−198.

Bradley, S.L., Hindmarsh, R.C.A., Whitehouse, P.L., Bentley, M.J., King, M.A., 2015. Low post- glacial rebound rates in the Weddell Sea due to Late Holocene ice-sheet readvance. Earth Planet Sci. Lett. 413, 79−89.

Briggs, R.D., Pollard, D., Tarasov, L., 2014. A data-constrained large ensemble analysis of Antarctic evolution since the Eemian. Quat. Sci. Rev. 103, 91−115.

Bromley, G.R.M., Hall, G., Stone, J., Conway, H., Todd, C., 2010. Late cenozoic deposits at reedy glacier, transantarctic mountains implications for former thickness of the west antarctic ice sheet. Quat. Sci. Rev. 29, 384−398.

Chmeleff, J., Blanckenburg, F., Kossert, K., Jakob, D., 2010. Determination of the ^{10}Be half-life by multicollector ICP-MS and liquid scintillation counting. Nucl. Instrum. Methods in Phys. Res. B 268, 192−199.

Depoorter, M., Bamber, J., Griggs, J., Lenaerts, J.T.M., Ligtenberg, S.R.M., van den Broeke, M.R., Moholdt, G., 2013. Calving fluxes and basal melt rates of Antarctic ice shelves. Nature 502, 89−92.

Dinniman, M.S., Klinck, J.M., Hofmann, E.E., 2012. Sensitivity of circumpolar deep water transport and ice shelf basal melt along the West Antarctic Peninsula to changes in the winds. J. Clim. 25, 4799−4816.

Dinniman, M.S., Asay-Davis, X.S., Galton-Fenzi, B.K., Holland, P.R., Jenkins, A., Timmermann, R., 2016. Modeling ice shelf/ocean interaction in Antarctica: a review. Oceanography 29, 144−153.

Dome Fuji Ice Core Project Members, Kawamura, K., Abe-Ouchi, A., Motoyama, H., Ageta, Y., Aoki, S., Azuma, N., Fujii, Y., Fujita, S., Fukui, K., Furukawa, T., Furusaki, A., Goto-Azuma, K., Greve, R., Hirabayashi, M., Hondoh, T., Hori, A., Horikawa, S., Horiuchi, K., Igarashi, M., Iizuka, Y., Kameda, T., Kanda, H., Kohno, M., Kuramoto, T., Matsushi, Y., Miyahara, M., Miyake, T., Miyamoto, A., Nagashima, Y., Nakayama, Y., Nakazawa, T., Nakazawa, F., Nishio, F., Obinata, I., Ohgaito, R., Oka, A., Okuno, J., Okuyama, J., Oyabu, I., Parrenin, F., Pattyn, F., Saito, F., Saito, T., Saito, T., Sakurai, T., Sasa, K., Seddik, H., Shibata, Y., Shinbori, K., Suzuki, K., Suzuki, T., Takahashi, A., Takahashi, K., Takahashi, S., Takata, M.,

Tanaka, M., Uemura, R., Watanabe, G., Watanabe, O., Yamasaki, T., Yokoyama, K., Yoshimori, T., Yoshimoto, T., 2017. State dependence of climatic instability over the past 720,000 years from Antarctic ice cores and climate modeling. Science Advances 3 (2), e1600446.

Golledge, N.R., Fogwill, C.J., Mackintosh, A.N., Buckley, K.M., 2012. Dynamics of the last glacial maximum antarctic ice sheet and its response to ocean forcing. Proc. Natl. Acad. Sci. U.S.A. 109, 16052—16056.

Golledge, N.R., Kowalewski, D., Naish, T., Levy, R., Fogwill, C., Gasson, E., 2015. The multi-millennial Antarctic commitment to future sea-level rise. Nature 526, 421—425.

Golledge, N.R., Keller, E.D., Gomez, N., Naughten, K.A., Bernales, J., Trusel, L.D., Edwards, T.L., 2019. Global environmental conse- quences of twenty-first-century ice-sheet melt. Nature 566, 65—72.

Gosse, J.C., Phillips, F.M., 2001. Terrestrial in situ cosmogenic nuclides: theory and application. Quat. Sci. Rev. 20, 1475—1560.

Hayashi, M., Yoshida, Y., 1994. Holocene raised beaches in the Lützow-Holm Bay region, East Antarctica. Memoir National Institute of Polar Research (special issue) 50, 49—84.

Hodgson, D.A., Noon, P.E., Vyverman, W., Bryant, C.L., Gore, D.B., Appleby, P., Gilmour, M., Verleyen, E., Sabbe, K., Jones, V.J., Ellis-Evans, J.C., Wood, P.B., 2001. Were the Larsemann Hills ice-free through the last glacial maximum? Antarct. Sci. 13, 440—454.

Igarashi, A., Numanami, H., Tsuchiya, Y., Harada, N., Fukuchi, M., Saitoh, T., 1995. Radiocarbon ages of molluscan shell fossils in raised beach deposits along the east coast of Lützow-Holm Bay, Antarctica, determined by accelerator mass-spectrometry. Proc. NIPR Symp. Polar Biol. 8, 154—162.

Igarashi, A., Numanami, H., Tsuchiya, Y., Fukuchi, M., 2001. Bathymetric distribution of fossil foraminifera within marine sediment cores from the eastern part of Lützow-Holm Bay, East Antarctica, and its paleoceanographic implications. Mar. Micropaleontol. 42, 125—162.

Ishikawa, T., Yanai, K., Matsumoto, Y., Kizaki, K., Kojima, S., Tatsumi, T., Kikuchi, T., Yoshikawa, M., 1977. Geological Map of Skarvsnes, Antarctica. Antarctic Geological Map Series, Sheet 6 and 7, National Institute of Polar Research, Tokyo, Japan.

Ivins, E.R., James, T.S., 2005. Antarctic glacial isostatic adjustment: a new assessment. Antarct. Sci. 17, 541—553.

Jacobs, S.S., Jenkins, A., Giulivi, C.F., Dutrieux, P., 2011. Stronger ocean circulation and increased melting under Pine Island Glacier ice shelf. Nat. Geosci. 4, 519—523.

Jenkins, A., Shoosmith, D., Dutrieux, P., Jacob, S., Kim, T.W., Lee, S.H., Ha, H.K., Stammerjohn, S., 2018. West Antarctic ice sheet retreat in the amundsen sea driven by decadal oceanic variability. Nat. Geosci. 11, 733—738.

Johnson, J.S., Bentley, M.J., Smith, J.A., Finkel, R.C., Rood, D.H., Gohl, K., Balco, G., Larter, R.D., Schaefer, J.M., 2014. Rapid thinning of pine island glacier in the early Holocene. Science 999—1001.

Johnson, J.S., Nichols, K.A., Goehring, B.M., Balco, G., Schaefer, J.M., 2019. Abrupt mid-Holocene ice loss in the western Weddell Sea Embayment of Antarctica. Earth Planet Sci. Lett. 518, 127—135.

Jones, R.S., Mackintosh, A.N., Norton, K.P., Golledge, N.R., Fogwill, C.J., Kubík, P.W., Christl, M., Greenwood, S.L., 2015. Rapid Holocene thinning of an East Antarctic outlet glacier driven by marine ice sheet instability. Nat. Commun. 6, 8910.

Jones, R.S., Norton, K.P., Mackintosh, A.N., Anderson, J.T.H., Kubik, P., Vockenhuber, C., Wittmann, H., Fink, D., Wilson, G.S., Golledge, N.R., McKay, R., 2017. Cosmogenic nuclides constrain surface fluctuations of an East Antarctic outlet glacier since the Pliocene. Earth Planet Sci. Lett. 480, 75—86.

Jones, R.S., Whitehouse, P.L., Bentley, M.J., Small, D.P., Dalton, A.S., 2019. Impact of glacial isostatic adjustment on cosmogenic surface-exposure dating. Quat. Sci. Rev. 212, 206—212.

Joughin, I., Smith, B.E., Medley, B., 2014. Marine ice sheet collapse potentially under way for the Thwaites Glacier basin, West Antarctica. Science 344, 735—738.

Kanamaru, T., Suganuma, Y., Oiwane, H., Miura, H., Miura, M., Okuno, J., Hayakawa, H., 2018. The weathering of granitic rocks in a hyper-arid and hy-pothermal environment: a case study from the Sør-Rondane Mountains, East Antarctica. Geomorphology 317, 62—74.

Kohl, C.P., Nishiizumi, K., 1992. Chemical isolation of quartz for measurement of in-situ-produced cosmogenic nuclides. Geochem. Cosmochim. Acta 56, 3583—3587.

Korschinek, G., Bergmaier, A., Faestermann, T., Gerstmann, U.C., Knie, K., Rugel, G., Wallner, A., Dillmann, I., Dollinger, G., Lierse von Gostomski, C., Kossert, K., Maiti, M., Poutivtsev, M., Remmert, A., 2010. A new value for the half-life of 10Be by Heavy-Ion Elastic Recoil Detection and liquid scintillation counting. Nucl. Instrum. Methods in Phys. Res. B 268, 187—191.

Lambeck, K., Rouby, H., Purcell, A., Sun, Y., Sambridge, M., 2014. Sea level and global ice volumes from the last glacial maximum to the Holocene. Proc. Natl. Acad. Sci. Unit. States Am. 111, 15296—15303.

Lifton, N., Sato, T., Dunai, T.J., 2014. Scaling in situ cosmogenic nuclide production rates using analytical approximations to atmospheric cosmic-ray fluxes. Earth Planet Sci. Lett. 386, 149—160.

Liu, Y., Moore, J.C., Cheng, X., Gladstone, R.M., Bassis, J.N., Liu, H., Wen, J., Hui, F., 2015. Ocean-driven thinning enhances iceberg calving and retreat of Antarctic ice shelves. Proc. Natl. Acad. Sci. U.S.A. 112, 3263—3268.

Mackintosh, A., White, D., Fink, D., Gore, D.B., Pickard, J., Fanning, P.C., 2007. Exposure ages from mountain dipsticks in Mac. Robertson Land, East Antarctica, indicate little change in ice-sheet thickness since the Last Glacial Maximum. Geology 35, 551—554.

Mackintosh, A., Golledge, N., Domack, E., Dunbar, R., Leventer, A., White, D.,

Pollard, D., DeConto, R., Fink, D., Zwartz, D., Gore, D., Lavoie, C., 2011. Retreat of the East Antarctic ice sheet during the last glacial termination. Nat. Geosci. 4, 195—202.

Mackintosh, A., Verleyen, E., O'Brien, P.E., White, D.A., Jones, R.S., McKay, R., Dunbar, R., Gore, D.B., Fink, D., Post, A.L., Miura, H., Leventer, A., Goodwin, I., Hodgson, D.A., Lilly, K., Crosta, X., Golledge, N.R., Wagner, B., Berg, S., van Ommen, T., Zwartz, D., Roberts, S.J., Vyverman, W., Masse, G., 2014. Retreat history of the east Antarctic ice sheet since the last glacial maximum. Quat. Sci. Rev. 100, 10—30.

Maemoku, H., Miura, H., Saigusa, S., Moriwaki, K., 1997. Stratigraphy of the late quaternary raised record of the late pleistocene beach deposits in the northern part of Langhovde, lutzow-holmbay, east Antarctica. Proc. NIPR symp. Antarct. Geosci. 10, 178—186.

Maemoku, H., Miura, H., Iwasaki, S., 2008. A possibility of glacial fluctuation in the East Antarctic Ice Sheet during mid Holocene deduced from the landforms and unconsolidated subsurface sediments. The 28th symposium on polar geo-sciences program and abstracts, 107P.

Miura, H., Maemoku, H., Seto, K., Moriwaki, K., 1998a. Late Quaternary East Ant-arctic melting event in the Soya Coast region based on stratigraphy and oxygen isotopic ratio of fossil molluscs. Polar Geosci. 11, 260—274.

Miura, H., Moriwaki, K., Maemoku, H., Hirakawa, K., 1998b. Fluctuations of the East Antarctic ice-sheet margin since the last glaciation from the stratigraphy of raised beach deposits along the Soya Coast. Ann. Glaciol. 27, 297—301.

Miura, H., Maemoku, H., Igarashi, A., Moriwaki, K., 1998c. Late Quaternary Raised Beach Deposits and Radiocarbon Dates of Marine Fossils Around Lützow-Holm Bay. Special Map Series of National Institute of Polar Research 6. National Institute of Polar Research, Tokyo.

Moriwaki, K., Yoshida, Y., 1983. Submarine topography of lutzow-holm bay, Antarctica. Mem.Natl. Inst. Polar res. Spec. Issue 28, 247—258.

Moriwaki, K., Iwata, S., Matsuoka, N., Hasegawa, H., Hirakawa, K., 1991. Weathering stage of till and glacial history of the central Sør-Rondane Mountains. Proc. NIPR Symp. Antarct. Geosci. 5, 99—111.

Moriwaki, K., Hirakawa, K., Hayashi, M., Iwata, S., 1992. Late cenozoic glacial history in the sør-rondane mountains, east Antarctica. In: Yoshida, Y., Kaminuma, K., Shiraishi, K. (Eds.), Recent Progress in Antarctic Earth Science. Terra Scientific Publishing Company, Tokyo, pp. 661—667.

Moriwaki, K., Iwata, S., Matsuoka, N., Hasegawa, H., Hirakawa, K., 1994. Weathering stage as a relative age of till in the central Sør-Rondane. Proc. NIPR Symp. Antarct. Geosci. 7, 156—161.

Nakai, Y., Kano, T., Yoshikawa, S., Ishikawa, T., Yanai, K., 1979. Explanatatory Text of Geological Map of Kjuka and Telen, Antarctica. Antarctic Geological Map Series, Sheet 8, National Institute of Polar Research. Japan, Tokyo.

Nakayama, Y., Menemenlis, D., Zhang, H., Schodlok, M., Rignot, E., 2018. Origin of circumpolar deep water intruding onto the amundsen and Bellingshausen sea continental shelves. Nat. Commun. 9, 3403.

Nishiizumi, K., 2004. Preparation of ^{26}Al ams standards. Nucl. Instrum. Methods phys. Res. Sect. B-beam interact. Mater. Atoms 223, 388—392.

Nishiizumi, K., Kohl, C.P., Arnold, J.R., Klein, J., Fink, D., Middleton, R., 1991. Cosmic ray produced ^{10}Be and ^{26}Al in Antarctic rocks: exposure and erosion history. Earth Planet Sci. Lett. 104, 440—454.

Nishiizumi, K., Imamura, M., Caffee, M.W., Southon, J.R., Finkel, R.C., McAninch, J., 2007. Absolute calibration of Be-10 AMS standards. Nucl. Instrum. Methods phys. Res. Sect. B-beam interact. Mater. Atoms 258, 403—413.

Ohzono, M., Tabei, T., Doi, K., Shibuya, K., Sagiya, T., 2006. Crustal movement of Antarctica and Syowa Station based on GPS measurements. Earth. Planets and Space 58, 795—804.

Okuno, J., Miura, H., 2013. Last deglacial relative sea level variations in Antarctica derived from glacial isostatic adjustment modelling. Geosci. Front 4, 623—632.

Osanai, Y., Toyoshima, T., Owada, M., Tsunogae, T., Hokada, T., Yoshimura, Y., Miyamoto, T., Motoyoshi, Y., Crowe, W.A., Harley, S.L., Kanao, M., Iwata, M., 2004. Geological Map of Skallen, Antarctica. Antarctic Geological Map Series, Sheet 40, National Institute of Polar Research. Japan, Tokyo.

Paolo, F.S., Fricker, H.A., Padman, L., 2015. Volume loss from Antarctic ice shelves is accelerating. Science 348, 327—331.

Peltier, W.R., Argus, D.F., Drummond, R., 2016. Space geodesy constrains ice age terminal deglaciation: the global ICE-6G_C (VM5a) model. J. Geophys. Res.-Solid Earth 120, 450—487.

Pritchard, H.D., Ligtenberg, S.R.M., Fricker, H.A., Vaughan, D.G., Van den Broeke, M.R., Padman, L., 2012. Antarctic ice-sheet loss driven by basal melting of ice shelves. Nature 484, 502—505.

Rignot, E., Mouginot, J., Scheuchl, B., 2011. Ice flow of the antarctic ice sheet. Science 333, 1427—1430.

Rignot, E., Jacobs, S., Mouginot, J., Scheuchl, B., 2013. Ice-shelf melting around Antarctica. Science 341, 266—270.

Rignot, E., Mouginot, J., Scheuchl, B., van den Broeke, M., van Wessem, M.J., Morlighem, M., 2019. Four decades of antarctic ice sheet mass balance from 1979—2017. Proc. Natl. Acad. Sci. 116, 1095—1103.

Sawagaki, T., Hirakawa, K., 1997. Erosion of bedrock by subglacial meltwater, Soya coast, east Antarctica. Geogr. Ann. 79, 223—238.

Sawagaki, T., Hirakawa, K., 2002a. Hydrostatic investigationons on subglacial meltwater: implications for the formation of streamlined bedforms and sub-glacial lakes, East Antarctica, Pol. Geosci. 15, 123—147.

Sawagaki, T., Hirakawa, K., 2002b. Terrestrial evidence of melting of the Antarctic ice sheet during the last glacial period. In: Gamble, John A., et al. (Eds.), Antarctica at the Close of a Millennium; Proceedings of the 8th International

Symposium on Antarctic Earth Sciences, vol. 35. Bulletin - Royal Society of New Zealand, pp. 404−414.

Schoof, C., 2007. Ice sheet grounding line dynamics: steady states, stability, and hysteresis. J. Geophys. Res.-Earth Surf. 112, F03S28.

Shepherd, A., Ivins, E.R., Geruo, A., Barletta, V.R., Bentley, M.J., Bettadpur, S., Briggs, K.H., Bromwich, D.H., Forsberg, R., Galin, N., Horwath, M., Jacobs, S., Joughin, I., King, M.A., Lenaerts, J.T.M., Li, J.L., Ligtenberg, S.R.M., Luckman, A., Luthcke, S.B., McMillan, M., Meister, R., Milne, G., Mouginot, J., Muir, A., Nicolas, J.P., Paden, J., Payne, A.J., Pritchard, H., Rignot, E., Rott, H., Sorensen, L.S., Scambos, T.A., Scheuchl, B., Schrama, E.J.O., Smith, B., Sundal, A.V., van Angelen, J.H., van de Berg, W.J., van den Broeke, M.R., Vaughan, D.G., Velicogna, I., Wahr, J., Whitehouse, P.L., Wingham, D.J., Yi, D.H., Young, D., Zwally, H.J., 2012. A reconciled estimate of ice-sheet mass balance. Science 338, 1183−1189.

Small, D., Bentley, M.J., Jones, R.S., Pittard, M.L., Whitehouse, P.L., 2019. Antarctic ice sheet palaeo-thinning rates from vertical transects of cosmogenic exposure ages. Quat. Sci. Rev. 206, 65−80.

Stone, J.O., Balco, G.A., Sugden, D.E., Caffee, M.W., Sass, L.C., Cowdery, S.G., Siddoway, C., 2003. Holocene deglaciation of Marie Byrd land, west Antarctica. Science 299, 99−102.

Suganuma, Y., Miura, H., Okuno, J., 2012. A new sampling technique for surface exposure dating using a portable electric rock cutter. Antarctic Record (Nankyoku Shiryo) 2, 85−90.

Suganuma, Y., Miura, H., Zondervan, A., Okuno, J., 2014. East Antarctic deglaciation and the link to global cooling during the Quaternary: evidence from glacial geomorphology and Be-10 surface exposure dating of the Sør Rondane Mountains, Dronning Maud Land. Quat. Sci. Rev. 97, 102−120.

Sugden, D.E., Balco, G., Cowdery, S.G., Stone, J.O., Sass, L.C., 2005. Selective glacial erosion and weathering zones in the coastal mountains of Marie Byrd Land, Antarctica. Geomorphology 67, 317−334.

Takada, M., Tani, A., Miura, H., Moriwaki, K., Nagatomo, T., 2003. ESR dating of fossil shells in the Lützow-Holm Bay region. East Antarctica. Quat. Sci. Rev. 22, 1323−1328.

Takano, Y., Tyler, J.J., Kojima, H., Yokoyama, Y., Tanabe, Y., Sato, T., Ogawa, N.O., Ohkouchi, N., Fukui, M., 2012. Holocene lake development and glacial-isostatic uplift at Lake Skallen and Lake Oyako, Lützow Holm Bay, East Antarctica, based on biogeochemical facies and molecular signatures. Appl. Geochem. 27, 2546−2559.

Thébault, E., Finlay, C.C., Beggan, C.D., Alken, P., Aubert, J., Barrois, O., Bertrand, F., Bondar, T., Boness, A., Brocco, L., Canet, E., Chambodut, A., Chulliat, A., Coïsson, P., Civet, F., Du, A., Fournier, A., Fratter, I., Gillet, N., Hamilton, B., Hamoudi, M., Hulot, G., Jager, T., Korte, M., Kuang, W., Lalanne, X., Langlais, B., Léger, J.-M., Lesur, V., Lowes, F.J., Macmillan, S., Mandea, M., Manoj, C., Maus, S., Olsen, N., Petrov, V., Ridley, V., Rother, M., Sabaka, T.J., Saturnino, D., Schachtschneider, R., Sirol, O., Tangborn, A., Thomson, A., Tøffner-Clausen, L., Vigneron, P., Wardinski, I., Zvereva, T., 2015. International geomagnetic reference field: the twelfth generation. Earth Planets Space 67−79.

Thoma, M., Jenkins, A., Holland, D., Jacobs, S., 2008. Modelling circumpolar deep water intrusions on the amundsen sea continental shelf, Antarctica. Geophys.

Res. Lett. 35, L18602.

Velicogna, I., Mohajerani, Y., Landerer F, A.G., Mouginot, J., Noel, B., Rignot, E., Sutterley, T., van den, Broeke M, Wessem, M. van, Wiese, D., 2020. Continuity of ice sheet mass loss in Greenland and Antarctica from the GRACE and GRACE Follow-On missions. Geophys. Res. Lett. 47, e2020GL087291.

Verleyen, E., Tavernier, I., Hodgson, D.A., Whitehouse, P.L., Kudoh, S., Imura, S., Heirman, K., Bentley, M.J., Roberts, S.J., Batist, M.D., Sabbe, K., Vyverman, W., 2017. Ice sheet retreat and glacio-isostatic adjustment in Lützow-Holm Bay, East Antarctica. Quat. Sci. Rev. 169, 85−98.

Watcham, E.P., Bentley, M.J., Hodgson, D.A., Roberts, S.J., Fretwell, P.T., Lloyd, J.M., Larter, R.D., Whitehouse, P.L., Leng, M.J., Monien, P., Moreton, S.G., 2011. A new Holocene relative sea-level curve for the South Shetland Islands, Antarctica. Quat. Sci. Rev. 30, 3152−3170.

Weber, M.E., Clark, P.U., Kuhn, G., Timmermann, A., Sprenk, D., Gladstone, R., Zhang, X., Lohmann, G., Menviel, L., Chikamoto, M.O., Friedrich, T., 2014. Millennial-scale variability in Antarctic ice-sheet discharge during the last deglaciation. Nature 510, 134.

Wessel, B., Huber, M., Wohlfart, C., Marschalk, U., Kosmann, D., Roth, A., 2018. Accuracy assessment of the global TanDEM-X digital elevation model with GPS data. ISPRS J. Photogramm. Rem. Sens 139, 171−182.

White, D.A., Fink, D., 2014. Late Quaternary glacial history constrains glacio-isostatic rebound in Enderby Land, East Antarctica. J. Geophys. Res.-Earth Surf. 119, 401−413.

White, D.A., Fink, D., Gore, D.B., 2011. Cosmogenic nuclide evidence for enhanced sensitivity of an East Antarctic ice stream to change during the last deglaciation. Geology 39, 23−26.

Whitehouse, P.L., Bentley, M.J., Milne, G.A., King, M.A., Thomas, I.D., 2012. A new glacial isostatic adjustment model for Antarctica: calibrated and tested using observations of relative sea-level change and present-day uplift rates. Geophys J. Bar Int. 190, 1464−1482.

Whitehouse, P.L., Bentley, M.J., Vieli, A., Jamieson, S.S.R., Hein, A.S., Sugden, D.E., 2017. Controls on last glacial maximum ice extent in the Weddell Sea embayment, Antarctica. J. Geophys. Res.-Earth Surf. 122, 371−397.

Whitehouse, P.L., Gomez, N., King, M.A., Wiens, D.A., 2019. Solid earth change and the evolution of the antarctic ice sheet. Nat. Commun. 10, 503.

Yamane, M., Yokoyama, Y., Miura, H., Maemoku, H., Iwasaki, S., Matsuzaki, H., 2011. The last deglacial history of Lützow-Holm Bay, East Antarctica. J. Quat. Sci. 26, 3−6.

Yamane, M., Yokoyama, Y., Abe-Ouchi, A., Obrochta, S., Sito, F., Moriwaki, K., Matuzaki, H., 2015. Exposure age and ice-sheet model constraints on Pliocene East Antarctic ice sheet dynamics. Nat. Commun. 6, 7016.

Yoshida, Y., 1983. Physiography of the prince olav and the prince harald coasts, east Antarctica. Memoirs of national Institute of polar Research. Ser. C. Earth Sci. 13, 1−83.

Zwartz, D., Stone, J., 1997. Cosmogenic Isotope Exposure Dating at Mt Riiser Larsen. Implications for Ice Sheet History. The 17th Symposium on Antarctic Geosciences, Program and Abstracts, 1997 Tokyo, National Institute for Polar Research, vol. 45. National institute for Polar Research, 45, Tokyo, 1997.